SENSITIVITY OF MODEL-GENERATED DAYTIME SURFACE HEAT FLUXES OVER SNOW TO LAND-COVER CHANGES

John E. Strack

NOAA Contract No. NA67RJ0152, Amendment 29
Roger A. Pielke and Glen E. Liston, Co-PIs

Colorado State University

DEPARTMENT OF ATMOSPHERIC SCIENCE

PAPER NO. 709

SENSITIVITY OF MODEL-GENERATED DAYTIME SURFACE HEAT FLUXES OVER SNOW TO LAND-COVER CHANGES

John E. Strack

Department of Atmospheric Science
Colorado State University
Fort Collins, Colorado
Fall 2001

Atmospheric Science Paper No. 709

ABSTRACT

SENSITIVITY OF MODEL-GENERATED DAYTIME SURFACE HEAT FLUXES OVER SNOW TO LAND-COVER CHANGES

Snow cover can significantly suppress daytime temperatures by increasing the surface albedo and limiting the surface temperature to 0°C. The strength of this effect is dependent upon how well the snow can cover, or mask, the underlying surface. In regions where tall vegetation protrudes through a shallow layer of snow the temperature-reducing effects of the snow will be suppressed since the protruding vegetation will absorb solar radiation and emit an upward turbulent heat flux. This means that an atmospheric model must have a reasonable representation of the land cover, as well as be able to correctly prognose snow depth, if an accurate simulation of surface heat fluxes, air temperatures, and boundary-layer structure is to be made. If too much vegetation protrudes through the snow then the surface sensible heat flux will be too large and the air temperatures will be too high.

In this study four simulations are run with RAMS 4.30 for a snow event that occurred in 1988 over the Texas Panhandle. The first simulation, called the control, is run with the most realistic version of the current land cover and the results verified against both ground stations and aircraft data. Simulations 2 and 3 use the default methods of specifying land cover in RAMS 4.29 and RAMS 4.30 respectively. The significance of these variations in land-cover definition are then examined by comparing with the control run. Finally, the last simulation is run with the land cover defined as all short grass, the natural cover for the region. The results of this study indicate that variations in the land-cover specification can lead to differences in sensible heat flux over snow as large as 80 W m^{-2}. These differences in sensible heat flux can then lead to differences in daytime temperatures by as much as 6°C. Also, the height of the afternoon boundary layer can vary as much as 200-300 m.

In addition, the results suggest that daytime temperatures are cooler over snow in the regions where short grass has been converted to cropland while they appear to be warmer over regions where shrubs have increased.

John E. Strack
Department of Atmospheric Science
Colorado State University
Fort Collins, Colorado 80523
Fall 2001

ACKNOWLEDGEMENTS

I would like to thank my advisor Dr. Roger Pielke Sr. for his expert guidance during the course of this research. I would also like to thank the other members of my committee, Dr. David Randall and Dr. Jorge Ramirez for their helpful suggestions and comments. Dr. Jimmy Adegoke and Dr. Joseph McFadden deserve special thanks for their help with processing the Landsat land-cover data. In addition, I must extend gratitude to Dr. Zhiqiang Gao for providing me with the 1 km resolution version of the Landsat data. I would like to thank Dr. Glen Liston, Dr. Robert Walko, and Dr. Joseph Eastman for their help in using RAMS. Thanks should be given to Dr. R. Louis Baumhardt and Dr. William Parton for their help with defining representative values for many of the vegetation parameters. I would like to acknowledge Mr. Ron Ruth for his help with obtaining the SSBLIM aircraft data. Finally, I would like to thank Ms. Dallas Staley for her help in preparing the text in final form.

This work was partially funded by a graduate fellowship from AMS/NASA's Earth Science Enterprise. Additional funding was provided by NOAA Contract No. NA67RJ0152 entitled "Parameterizing Subgrid-Scale Snow-Cover Heterogeneities for Use in Regional and Global Climate Models." The NCAR-NCEP reanalysis, U.S. Summary of the Day snow data, upper-air observations, and surface observations used to initialize these simulations are provided by the Data Support Section Scientific Computing Division at NCAR. NCAR is supported by grants from the National Science Foundation.

TABLE OF CONTENTS

LIST OF FIGURES

LIST OF TABLES

Chapter 1

INTRODUCTION

There has been a considerable amount of research illustrating how snow can significantly reduce daytime temperatures by as much as 10°C on time scales of days to months (Namias 1985; Cohen and Rind 1991; Baker et al. 1992; Leathers and Robinson 1993; and Ellis and Leathers 1998). Snow cover reduces daytime temperatures by increasing the net surface albedo and reducing the maximum attainable surface temperature. First of all, the higher surface albedo reduces the amount of incoming solar radiation which can be absorbed meaning less energy will be available to heat the surface and nearby air. Secondly, the temperature of the snow is limited to 0°C or less. Once the snow temperature reaches 0°C the remaining energy can only be used for melting. These two effects combine to produce a surface that is significantly cooler than its snow-free counterpart under the same ambient conditions.

The strength of these cooling effects is obviously dependent upon the extent to which the snow is able to cover, or mask, the land surface. When tall vegetation, such as trees or shrubs, protrude through a shallow snow cover the albedo increasing effect of the snow is reduced; see Figure 1.1. Furthermore, the protruding vegetation is capable of warming to temperatures greater than the 0°C limit of snow allowing for a greater surface sensible heat flux. In contrast, the same shallow snow cover may be able to completely bury short vegetation such as grass or crop stubble, enabling the full temperature reducing effects of the snow to be realized. In the case of the study by Baker et al. (1992) the mean reduction in daily maximum temperature was 8.4°C when the surface was completely masked and 6.5°C when the surface was partially masked by snow.

Some modeling studies have also looked at the influence of protruding vegetation on temperatures and heat fluxes over snow. The sensitivity of surface heat fluxes and low-level

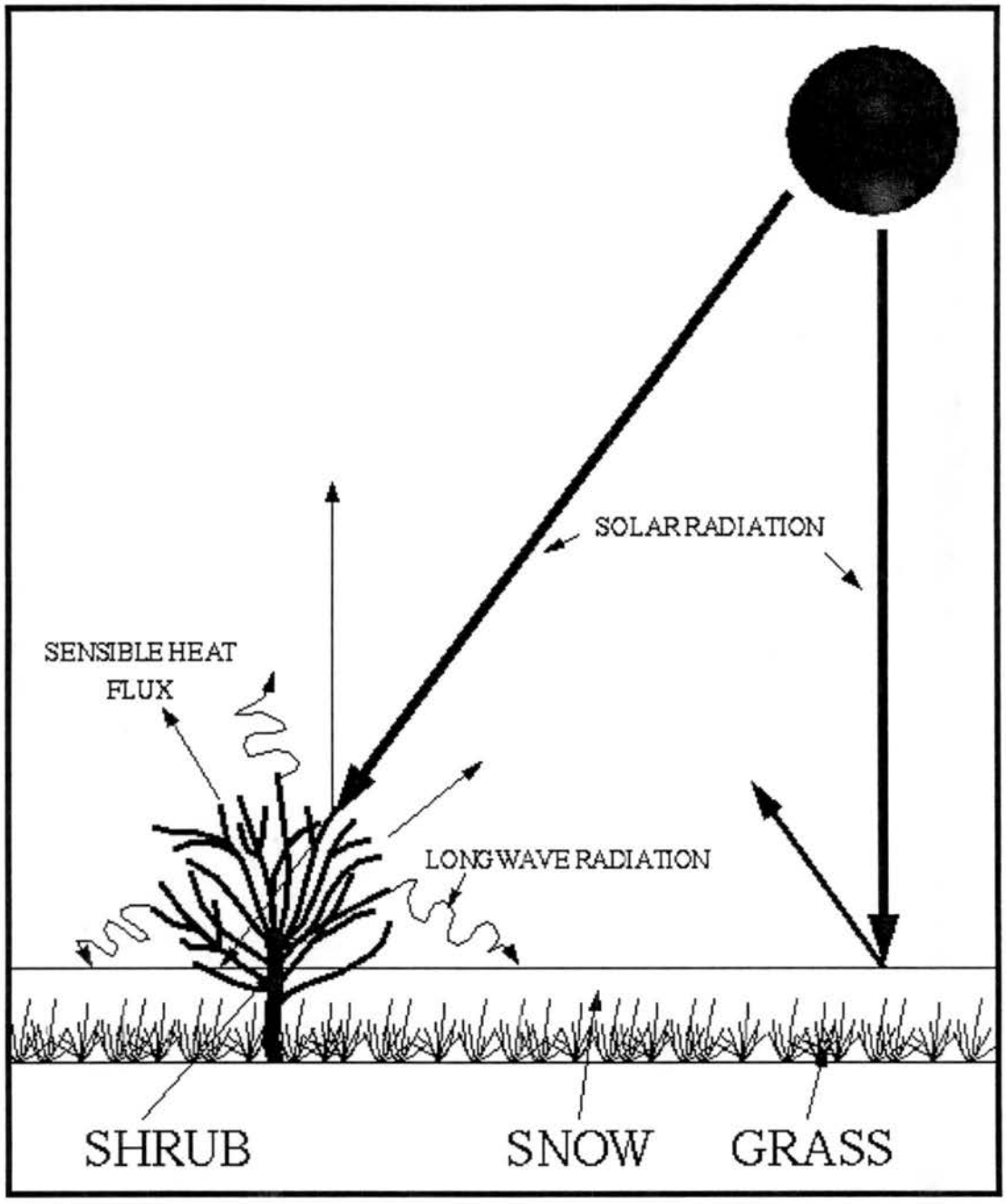

Figure 1.1: Schematic showing the key energy exchange mechanisms over a snow cover interspersed with protruding shrubs.

air temperature to masking of the land cover by snow has been examined for the boreal forests of the northern hemisphere by Thomas and Rowntree (1992) and Viterbo and Betts (1999). In addition, Greene et al. (1999) illustrated the importance of the albedo reduction by forests in the Rocky Mountains. Thomas and Rowntree (1992) represented the removal of the boreal forests as an increase in the maximum winter and spring albedo over these regions in the United Kingdom Meteorological Office (UKMO) general circulation model. The albedo of the boreal forest regions in the winter and spring is generally much lower than that of snow since the dark trees easily protrude through the snow pack. The removal of these forests would lead to a significant increase in the surface albedo of the region. In the Thomas and Rowntree (1992) study the increase in albedo due to forest removal led to a reduction in surface sensible heat fluxes, air temperatures, and precipitation during the spring. Viterbo and Betts (1999) showed that a reduction in the boreal forest deep snow albedo in the European Center for Medium-Range Weather Forecasts (ECMWF) model significantly reduced the model's cold low-level temperature bias present in the boreal forest region during the spring. The ECMWF model had been neglecting the reduction in albedo due to the protruding forest and assigned a value for the surface albedo that was too high leading to the cold bias in low-level temperatures.

Finally, Greene et al. (1999) showed with the ClimRAMS model that surface sensible heat fluxes and low-level air temperatures were reduced during late winter and early spring when forest areas were replaced with grassland in the Rocky Mountains.

Considering the previous discussion, one should be able to see that the ability of an atmospheric model to correctly simulate daytime temperatures over snow will be dependent upon the accuracy of the land-cover definition. If the land cover in a model is defined to be 1 m tall shrubs when in fact 5 cm crop stubble is present then one would expect the model to overpredict the surface heat flux over a 15 cm deep snow cover. The overpredicted surface heat flux would in turn lead to higher near-surface air temperatures and a deeper afternoon boundary layer.

This study seeks to illustrate the sensitivity of model-simulated daytime temperatures over snow to the underlying land cover. The Colorado State University Regional

Atmospheric Modeling System (CSU-RAMS; Pielke et al. 1992) vs. 4.30 is used to run four 12-hour long simulations centered in the Texas Panhandle. The first three will each use a different method of specifying the present day land cover. The first simulation, which is considered the control, uses the 30 m resolution Landsat Thematic Mapper (TM) derived National Land Cover Data (NLCD) to define the present day land cover (Vogelmann et al. 1998). Simulations 2 and 3 utilize the 1 km resolution Advanced Very High Resolution Radiometer (AVHRR) derived Olson Global Ecosystem (OGE) land cover data to define the present day land cover (Olson 1994a,b). Finally, in simulation 4 the land cover will be defined as all short grass, the predominant pre-settlement vegetation in the southern U.S. Plains. The evolution of sensible and latent heat fluxes, near-surface air temperature, snow depth, and boundary-layer structure as simulated by the model is then examined for each of the land-cover definitions. In contrast to the modeling studies mentioned above, this experiment focuses on the effects of protruding vegetation with relatively small stature, such as shrubs, on the boundary layer. In addition, this study examines these effects in a mid-latitude and relatively low altitude region. The research is also different since it explores the significance of not only changes in land cover in a region but also the sensitivity to different methods of specifying the current land cover. The overall goal here is to highlight the necessity of properly representing the land cover in numerical weather and climate models and how slight variations between different land-cover data sets can lead to significant differences in model results. The study also provides further evidence of how changes in land cover over time can lead to changes in low-level air temperatures and hence the need for treating the land surface as a dynamic component of any climate system model. Finally, the results of this work will further show the need for considering land-cover changes when examining long-term temperature records from surface stations for trends.

Chapter 2 explains the design of the experiment and describes in detail the Land Ecosystem-Atmosphere Feedback model vs. 2 (LEAF-2) land-surface parameterization used by RAMS. An extensive discussion of the control run configuration is given in Chapter 3, followed by a comparison of the control run results with observations and a discus-

sion of the other simulations in Chapter 4. Finally, Chapter 5 contains a summary and recommendations for future work.

Chapter 2

EXPERIMENTAL DESIGN

2.1 Experiment Methodology

RAMS 4.30 with LEAF-2 is used to simulate daytime temperatures over a 5 to 30 cm deep cover of melting snow in the Texas Panhandle on March 18, 1988. This particular event was chosen because of its location in a region where significant land-use change has occurred, as well as the availability of heat flux and albedo measurements from the Snow Shading Boundary Layer Interaction Measurement Program (SSBLIM) described in Cramer (1988). The region is also ideal because a large fraction of it is defined as a mixed shrub and grass category in the OGE AVHRR-derived data set which is the standard land-cover set for LEAF-2. This category presents a problem since there is no such corresponding mixed class in the Biosphere Atmosphere Transfer Scheme (BATS) (Dickinson et al. 1986) that LEAF-2 cross references the Olson classes with. The mixed class is either defined as all shrubs, as was the case in RAMS 4.29, or all grass, as in RAMS 4.30. As is shown later this has significant consequences for daytime temperatures over snow. The first step is to run a simulation with the best land-cover representation available and compare the results to the available observations. This simulation, which we will call the control, will be the baseline that we compare the results of all subsequent simulations. We consider the 30 m resolution Landsat TM-derived land cover to be the best for the Texas Panhandle since it distinguishes between the grass and shrubs, allowing for separate fractions for each to be defined in LEAF-2, and appears to give a better fraction of crop land. After demonstrating with the control run that the model can reasonably reproduce available observations we make the assumption that the results from subsequent simulations with land-cover modifications are a reasonable representation of what would

Table 2.1: List of the four simulations.

Simulation	Control Run	Simulation 2	Simulation 3	Simulation 4
Land Cover	Landsat TM	AVHRR-shrub/grass mix defined as all shrub	AVHRR-shrub/grass mix defined as all short grass	Pre-Settlement land cover, all short grass

actually occur if such land-cover changes occurred. The second simulation will be run using the 1 km AVHRR-derived land cover with the grass and shrub mixture described above classified as all shrubs in LEAF-2, and the third simulation will be run with this class defined as all short grass. Finally, the fourth simulation will be run with the entire land cover defined simply as all short grass, a situation that represents the pre-settlement, or natural state of the land. The four simulations are listed in Table 2.1 for reference.

We expect that representing the shrub/grass mixture as all shrubs will lead to higher daytime temperatures. The tall shrubs protrude through the snow, and thus are warmed by the sun. As a result upward turbulent sensible heat flux occurs. Since the fraction of the shrubs will be much larger in this case the afternoon air temperatures will be correspondingly higher. The opposite situation is expected for simulation 3 where the shrub/grass mix will be treated as all short grass. In this case the fraction of shrubs will be smaller leading to a reduction in afternoon temperatures. From simulation four we expect to find that an increase in the shrub population in this region since pre-settlement times may produce higher daytime temperatures over snow. Also, cooler temperatures are expected over the crop stubble areas since the stubble is generally shorter than the natural grass.

2.2 LEAF-2 Description

LEAF-2 is the land-surface parameterization used by RAMS 4.30. Much of the following description, which is included for completeness, is taken from Walko et al. (2000). LEAF-2 consists of the soil, snow or temporary surface water, vegetation, and canopy air. Each grid cell in RAMS is broken down into a permanent surface water patch and an

additional user defined number of land-cover type patches. The permanent surface water patch represents the fraction of the grid cell that is occupied by rivers, lakes, or ocean while the other patches represent the fractions of the most dominant land-cover types. LEAF-2 is run separately for each of the patches and the influence of each patch on the lowest atmospheric level in RAMS is weighted according to its fractional area. There is no direct communication between the patches, however, they influence each other indirectly through their effects on the lowest atmospheric level in RAMS. This fractional break down of the land surface allows the land cover, which often has fine spatial structure, to be represented at relatively higher resolution than the more computationally expensive atmospheric grid. A qualitative description of each of the major components of LEAF-2 is given in the sections that follow. Equations for some of the quantities and processes most relevant to the this study are also given. A more comprehensive listing of the equations in LEAF-2 are given in Appendix D of Pielke (2001).

2.2.1 Soil

The soil in LEAF-2 is broken down into layers, the number and thickness of which are defined by the user. Soil moisture content in the surface layer is determined from percolation of temporary surface water (snowmelt), percolation of liquid moisture from the surface layer to the next layer below, evaporation to the canopy air, removal through transpiration by plants, and runoff simulated by TOPMODEL (Beven and Kirkby 1979; Beven 1982; Sivapalan et al. 1987). The moisture in the remaining layers below the surface is calculated from the vertical liquid moisture flux divergence, removal through transpiration by plants, and sub-surface runoff as simulated by TOPMODEL.

LEAF-2 does not directly prognose soil temperature but rather diagnoses it from soil internal energy. The soil internal energy is defined relative to a value of 0 for soil with completely frozen moisture at 0°C. The equation for soil internal energy, in units of J m^{-3}, is:

$$Q_g = W_g f_i C_i T_g + W_g f_l \left(C_l T_g + L_{il}\right) + C_g M_g T_g \tag{2.1}$$

where:

C_g = specific heat of dry soil J kg^{-1} K^{-1}

C_i = specific heat of ice J kg^{-1} K^{-1}

C_l = specific heat of liquid water J kg^{-1} K^{-1}

f_i = ice fraction (by mass)

f_l = liquid water fraction (by mass)

L_{il} = latent heat of fusion J kg^{-1}

M_g = mass of dry soil per cubic meter of total volume kg m^{-3}

W_g = soil water content kg m^{-3}.

Here soil temperature, T_g, is in °C, and f_i and f_l are the ice and liquid water fractions, respectively, relative to the total mass of water in the soil. At initialization time each soil layer is assigned an initial temperature from which Q_g is computed with 2.1. After each time step the soil internal energy in the surface soil layer is updated using the net radiation, conduction from the next soil layer below, the turbulent sensible heat flux to the canopy air, (or, when snow is present, conduction between the soil and bottom snow layer), latent heat due to evaporation from the surface, and the net flux divergence of the energy carried by percolating water. In the soil layers below the surface the internal energy is updated based on the conduction between adjacent layers and the energy carried by the net flux divergence of percolating moisture in the layer. After Q_g is updated the new soil temperature and liquid/ice fractions are diagnosed from 2.1.

2.2.2 Snow

Snow is considered to be the frozen part of the temporary surface water component in LEAF-2. Multiple snow layers are allowed, and as in the case of soil, internal energy is prognosed for each of them. The temperature of the snow layer is then diagnosed from the internal energy. Equation 2.2, shown below, defines the snow internal energy in J kg^{-1} in a similar fashion as 2.1 does for soil;

$$Q_s = f_i C_i T_s + f_l \left(C_l T_s + L_{il} \right) \tag{2.2}$$

where T_s = the snow temperature in degrees C.

This gives the internal energy relative to a reference state of all ice at 0°C, at which point Q_s is 0. Temperature is again in °C in this equation. At each time step, Q_s in

the top most snow layer is updated by the net radiation, conduction of heat from the layer below, energy carried by the net flux divergence of liquid water percolation, and latent heat flux from evaporation and sublimation to canopy air. In intermediate layers Q_s is updated from the absorption of transmitted solar radiation, conduction between adjacent layers, and by energy carried by the net flux divergence of percolating liquid water. Finally, for the bottom most snow layer Q_s is updated from absorbed transmitted solar radiation, energy carried by the net flux divergence of percolating liquid water, and conduction of heat from both the soil surface and the next snow layer above. As with the soil a new temperature, and the fractions of liquid and ice, are computed from the new internal energy.

By default in LEAF-2 the snow albedo is assigned a maximum value of 0.5 when in the form of all ice. The albedo decreases linearly to the value for wet soil (0.14) as the liquid fraction increases to 1. For this study the same linear decrease to 0.14 is used but the maximum albedo has been increased to 0.6. Ample documentation exists (Hartmann 1994; Sellers 1965) supporting such a value for the snow albedo. The value of 0.6 was chosen since it agrees well with the albedo measurements from the SSBLIM study. In reality, the albedo of snow has a spectral dependence where the albedo decreases with longer wavelengths. However, in LEAF-2 the albedo is held constant across all wavelengths for solar radiation. The longwave emissivity of the snow is assumed to be unity.

In the current implementation of LEAF-2 the snow depth is updated each time step by the amount of snow reaching the ground and snowmelt. The depth also decreases each time due to a prescribed compression rate as shown in the following equation:

$$z_s = z_s \left[1 - \frac{\Delta t}{1 \times 10^5} \right] \tag{2.3}$$

where Δt is the time step in s, and z_s is snow depth in m.

The amount of snowmelt is calculated in terms of mass per unit area and the depth loss is computed as the depth this mass would fill if in the form of liquid water. For this study the snow depth is simply diagnosed from the ice and liquid water fractions with the density of the ice fraction remaining constant with time. Each time step the

depths of liquid water and ice are computed and summed to get the total snow depth. The density of the ice fraction of the snow is assumed to remain constant at its initial value. The assumption of a constant value for the ice fraction density is not too bad for this situation since the duration of the simulation is so short and the snow is relatively shallow. Internal compression from the weight of the snow itself will not be very large in this case. This alternative method for determining snow depth evolution was utilized for this study because the standard method does not allow for significant differences in snow depth due to differences in the rate of conversion of ice to liquid. Most of the depth change comes from the prescribed compression given by Equation 2.3 which has no dependence upon conversion of ice to liquid.

2.2.3 Vegetation

In RAMS 4.30 LEAF-2 cross references all vegetation types either to one of the 18 BATS categories or in a few cases to a wooded grassland or urban category that physical parameters have been defined for. The vegetation physical parameters used by LEAF-2 are albedo, leaf area index (LAI), vegetation fraction, emissivity, roughness length, displacement height, and root depth. The LAI and vegetation fraction are allowed to vary on a prescribed seasonal basis. Vegetation fraction represents the fraction of the ground surface that is covered by vegetation. The rest of the surface is considered to be bare soil.

The vegetation temperature is prognosed from the amount of energy exchanged between the net radiation, turbulent sensible heat flux, latent heat flux from evaporation of intercepted precipitation, latent heat flux from the process of transpiration, and energy carried by intercepted precipitation. The net radiation is the sum of absorbed solar radiation and longwave radiation from the atmosphere and the ground or snow surface. The equations for the radiation exchanges as well as the sensible heat flux are given below.

The solar radiation absorbed by the vegetation is given by:

$$S_v = R_{s\downarrow}\Gamma_s \left[1 - \alpha_v + \alpha_s \left(1 - \Gamma_s\right)\right] \tag{2.4}$$

$R_{S\downarrow}$ = incoming solar radiation at the bottom of the atmosphere W m^{-2}

Γ_s = vegetation fraction corrected for snow depth

α_s = snow albedo

α_v = vegetation albedo.

The vegetation fraction is assumed to decrease linearly towards zero as snow depth approaches the height of the vegetation; see Equation 2.5 below.

$$\Gamma_s = \max\left[0, \Gamma\left(1 - \frac{z_s}{z_v}\right)\right] \tag{2.5}$$

Γ = vegetation fraction

z_s = snow depth m

z_v = vegetation height m.

Next, the longwave radiation exchange between the vegetation and atmosphere is given by:

$$F_{rva} = \epsilon_v \sigma T_v^4 \Gamma_s \left[1 + (1 - \Gamma_s)(1 - \epsilon_{gs})\right] - R_{L\downarrow} \Gamma_s \left[\epsilon_v + (1 - \Gamma_s)(1 - \epsilon_{gs})\right] \tag{2.6}$$

$R_{L\downarrow}$ = downward longwave radiation at the bottom of the atmosphere W m^{-2}

T_v = temperature of vegetation K

ϵ_v = emissivity of vegetation

ϵ_{gs} = emissivity of ground or snow

σ = Stephan-Boltzmann constant.

The longwave radiation exchange between the snow and vegetation is given by:

$$F_{rsv} = \epsilon_v \epsilon_s \sigma \Gamma_s \left[T_s^4 - T_v^4\right] \tag{2.7}$$

T_s = temperature of snow K

ϵ_s = emissivity of snow.

Finally, the longwave radiation exchange between the bare ground and the vegetation is:

$$F_{rgv} = \epsilon_v \epsilon_g \sigma \Gamma \left[T_g^4 - T_v^4\right] \tag{2.8}$$

ϵ_g = emissivity of the ground

T_g = temperature of the ground K.

The sensible heat flux between the vegetation and the canopy air is given by (Lee 1992):

$$F_{hvc} = 2.2\Upsilon_s \frac{C_p \rho_a (T_v - T_c)}{r_b} \tag{2.9}$$

C_p = specific heat of air J kg^{-1} K^{-1}

T_c = canopy air temperature K

r_b = resistance between canopy air and vegetation surface s m^{-1}

Υ_s =leaf area index corrected for snow depth

ρ_a = air density kg m^{-3}.

The leaf area index is allowed to linearly approach zero as the snow depth approaches the height of the vegetation, just as in the case of vegetation fraction. The 2.2 factor arises from the need to include both sides of the leaves and the assumption that the stem area is equal to about 10% of the one sided leaf area. Equation 2.9 is used for all vegetation types in this case except the deciduous shrubs. LEAF-2 in its present state can not accurately produce sensible heat fluxes from vegetation that is completely bare of leaves, since it is based on leaf area index. In order to get around this the sensible heat flux from the shrubs is modeled as being equal to the net radiation absorbed by the branches as in Otterman et al. (1993). This assumes that the heat capacity of the shrubs is very small and that there is no cooling due to latent heat of evaporation. Cooling of the shrubs by latent heat of evaporation will be negligible in this situation since they are dormant and dry.

2.2.4 Canopy Air

The canopy air is considered to be the air in immediate contact with the vegetation and surface. The canopy air temperature is prognosed from turbulent sensible heat flux from the vegetation and ground or snow, and the sensible heat flux to the lowest atmospheric model level. The moisture content of the canopy air is prognosed from the rate of moisture exchange between the ground or snow, intercepted precipitation on vegetation, transpiration, and the lowest atmospheric model level. The equations for heat and moisture exchange involving the canopy air (taken from Lee 1992) that are most relevant to this study are listed below.

The sensible heat flux from the vegetation to the canopy air has already been listed above and will not be repeated. Below are the equations for sensible heat flux from the snow and ground to canopy air respectively.

$$F_{hsc} = \frac{C_p \rho_a (T_s - T_c)}{r_d} \tag{2.10}$$

r_d = resistance between ground and canopy air s m^{-1}.

$$F_{hgc} = \frac{C_p \rho_a (T_g - T_c)}{r_d} \tag{2.11}$$

The moisture flux due to evaporation from the soil and snow to canopy air are respectively:

$$F_{wgc} = \frac{\rho_a (\chi_g - \chi_c)}{r_d} \tag{2.12}$$

χ_g = water vapor mixing ratio at the ground surface kg kg^{-1}

χ_c = water vapor mixing ratio of the canopy air kg kg^{-1}.

$$F_{wsc} = \frac{\rho_a (\chi_s - \chi_c)}{r_d} \tag{2.13}$$

χ_s = water vapor mixing ratio at equilibrium with snow surface kg kg^{-1}.

Finally, the sensible heat and moisture fluxes from the canopy air to the lowest model level are given below:

$$F_{hca} = -C_p \rho_a u_* T_* \tag{2.14}$$

$$F_{wca} = -\rho_a u_* \chi_* \tag{2.15}$$

The flux parameters for momentum, temperature, and water vapor mixing ratio, (u_*, T_*, and χ_* respectively), are based on surface similarity theory as described in Louis (1981).

Chapter 3

MODEL CONFIGURATION

3.1 Atmospheric Initialization

Three nested grids, as shown in Figure 3.1, are used in this study. The outer most coarse grid covers most of North America and has horizontal grid intervals of 200 km. The second grid covers a large part of the central U. S. and has horizontal intervals of 50 km, while the innermost grid is centered on the Texas Panhandle with horizontal grid intervals of 10 km. On the two outer grids vertical grid intervals range from 30 m near the surface to 1000 m above the 5 km level. Vertical grid intervals on the fine grid range from 10 m in the first 120 m to 1000 m above the 5 km level. The two coarse grids have a total of 47 levels reaching an altitude of about 18 km. The fine grid has 59 levels which also extend to about 18 km.

The model is initialized at 12 UTC 18 March 1988 with the NCAR-NCEP reanalysis (Kalnay et al. 1996) along with available surface and rawinsonde observations. The simulation is run for 12 hours. The Smagorinsky (Smagorinsky et al. 1965) and Mellor-Yamada (Mellor and Yamada 1982) turbulence schemes are used for horizontal and vertical diffusion, respectively. Both shortwave and longwave radiation are parameterized using the Chen and Cotton (Chen and Cotton 1983) routine. The boundaries of the outermost grid are nudged toward the NCAR-NCEP reanalysis at the halfway point of the simulation.

3.2 Land-Cover Specification

For all simulations the 1 km AVHRR-derived OGE land-cover data is used to specify the land cover in the regions outside of the fine grid. In the control simulation a 1 km resolution version of the 30 m TM-derived NLCD is used to define the land cover in the

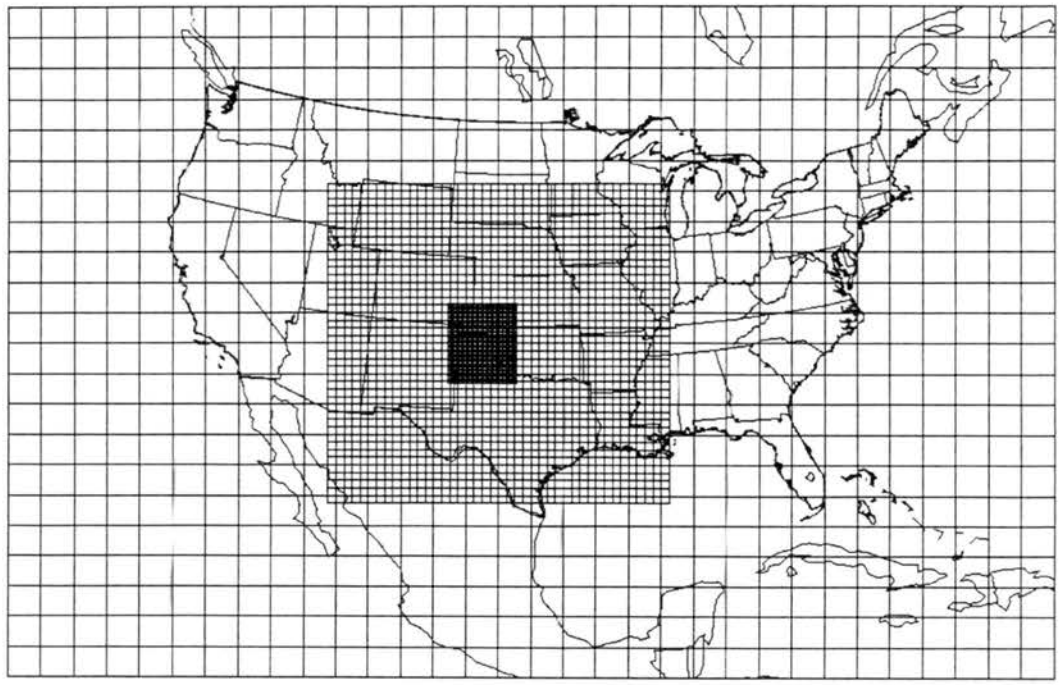

Figure 3.1: Atmospheric grids used for all four of the simulations.

region of the fine domain. The 1 km data contains the percentage of each 1 km cell occupied by each of the 21 NLCD land-cover types. This version of the data was used because the original 30 m version required too much computer memory to process. Some spatial resolution is lost by using the 1 km version, but this is insignificant in this case since the finest RAMS grid has increments of 10 km. The important thing is that an accurate measure of the fractional area of each land-cover type can be determined in each of the RAMS grid cells.

There is a considerable amount of crop land in the Texas Panhandle. The primary crops grown in this region are grain sorghum, winter wheat, cotton, and corn. During mid-March sorghum, corn, and cotton fields are typically stubble while the winter wheat is growing. The Landsat data defines the crop land as either row crops or small grains. Corn and cotton are the two dominant row crops in the region. The row crop fractions are considered to be stubble in the winter.

Treating the small grain category is more tricky since part of this is winter wheat which is green in contrast to sorghum, the other small grain in the area, which is a summer crop and thus stubble in March. A typical crop rotation used in this region is

the wheat-sorghum-fallow rotation described in Jones and Popham (1997). Taking this into consideration 1/3 of the small grain area is estimated to be winter wheat and the other 2/3 is stubble. Crop stubble in this region is typically flat from tillage practices and weathering by mid-March (personal communication with R. Louis Baumhardt[1]). Two new vegetation classes were created in LEAF-2 to represent crop stubble and winter wheat. In the case of the stubble the albedo is set to 0.25, a typical value for dry vegetation (Hartmann 1994), the LAI is set to 1, the vegetation fraction and canopy height are set to 0.6 and 0.05 m respectively (personal communication with R. Louis Baumhardt). The LAI of 1 for crop stubble was estimated from the rule of thumb that LAI is roughly equal to the number of leaves that a straight line dropped down from the canopy top to the surface would intersect (Hartmann 1994). The remaining parameters were left the same as those for the crop/mixed farming class in BATS. The winter wheat category was derived from the BATS short grass class, with the exceptions that the albedo was decreased to 0.2, a typical value for green vegetation (Hartmann 1994), the LAI was reduced from the BATS value to 1.3 (as estimated for short grass from personal communication with William Parton[2]), and the canopy height was reduced to 0.1 m (personal communication with R. Louis Baumhardt).

The dominant noncrop land-cover types in the Panhandle are short grass and shrubs. The most common short grass types are blue grama and buffalograss while the dominant shrub is honey mesquite (Scifres 1980). Typical heights for buffalograss range from 0.05 to 0.25 m while those for blue grama are 0.2 to 0.7 m (Hatch and Pluhar 1993). With this in mind an average height of 0.2 m is given to the short grass category. The LAI is assigned a value of 1.3 (personal communication with William Parton). Albedo is set to 0.25, a typical value for dry vegetation (Hartmann 1994). The other parameters for short grass are left the same as the defaults in LEAF-2. Honey mesquite shrubs are deciduous

---

[1]Dr. R. Louis Baumhardt is a soil scientist at the United States Department of Agriculture Agricultural Research Service (USDA-ARS) Conservation and Production Research Laboratory in Bushland, TX.

[2]Dr. William Parton is a professor in the Natural Resource Ecology Lab (NREL) at Colorado State University.

Table 3.1: The key physical parameters for the vegetation types most prevalent in the study area.

	LAI	Veg. Fraction	Canopy Height	Albedo
Short Grass	1.3	0.74	0.20 m	0.25
Shrubs	0.1	0.50	1.60 m	0.15
Stubble	1.0	0.60	0.05 m	0.25
Winter Wheat	1.3	0.74	0.10 m	0.20

and have typical heights of 1-4 m (Hatch and Pluhar 1993). The LAI of the shrubs is set to 0.1 since most of the leaves will be off in mid March, and the vegetation fraction is reduced to 0.5 (personal communication with Parton). The albedo has been set to 0.15, a reduction from the default in the shrub category of 0.20, in response to the lower LAI value used here. The rest of the shrub parameters are left the same as the defaults in LEAF-2. Table 3.1 summarizes the key physical parameters for the vegetation types that are most prevalent in the study area.

3.3 Snow-Cover Initialization

Snow cover is initialized using a combination of U.S. Summary of the Day (USSOD) observations and visible satellite imagery. The first step was to select all USSOD stations with observation times within 2 hours of the model start time of 12 UTC. Those stations in the region of interest are shown in Figure 3.2. The snow depths from these stations were then interpolated on to the three RAMS grids. The area distribution of the snow over the region of interest on the fine grid was then manually refined with the aid of visible satellite imagery; see Figure 3.3. In particular the fork in the snow field shown in the satellite image was not reproduced in the interpolation due to sparseness of data and so it was added manually; see Figure 3.4.

The initial density of the snow was set to 100 kg m^{-3}, a value determined from a liquid water measurement at Amarillo, TX six hours before model start time of 12 UTC. The air temperature across the snow region was well below freezing, between –11 and –5°C, and so the snow was assumed to be all ice at initialization. Since skies were clear

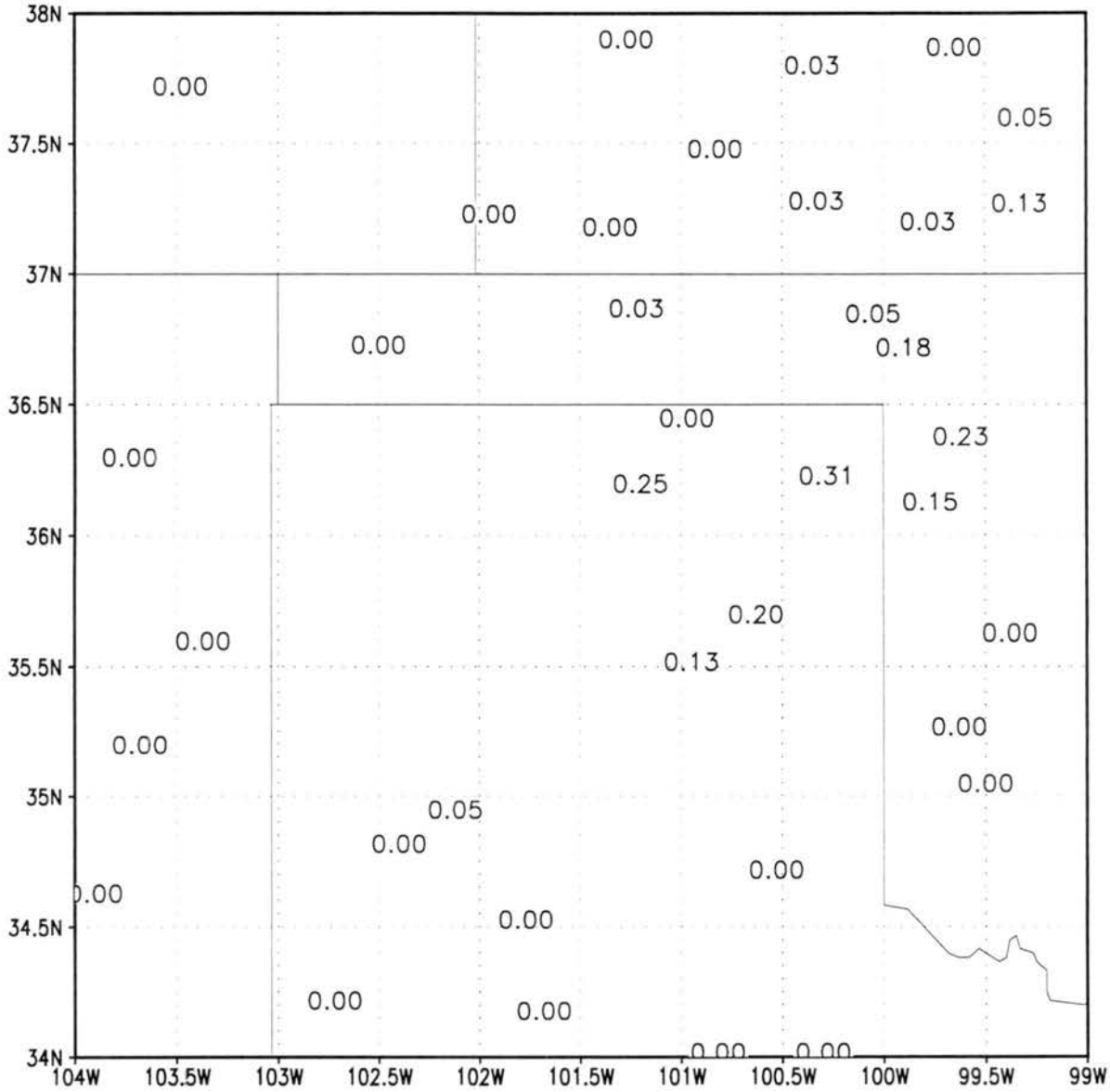

Figure 3.2: USSOD stations used for initializing the snow depth. Values represent the observed snow depth in meters.

Figure 3.3: Snow cover as shown by 1 km resolution visible satellite imagery at 13:48 UTC 18 March 1988.

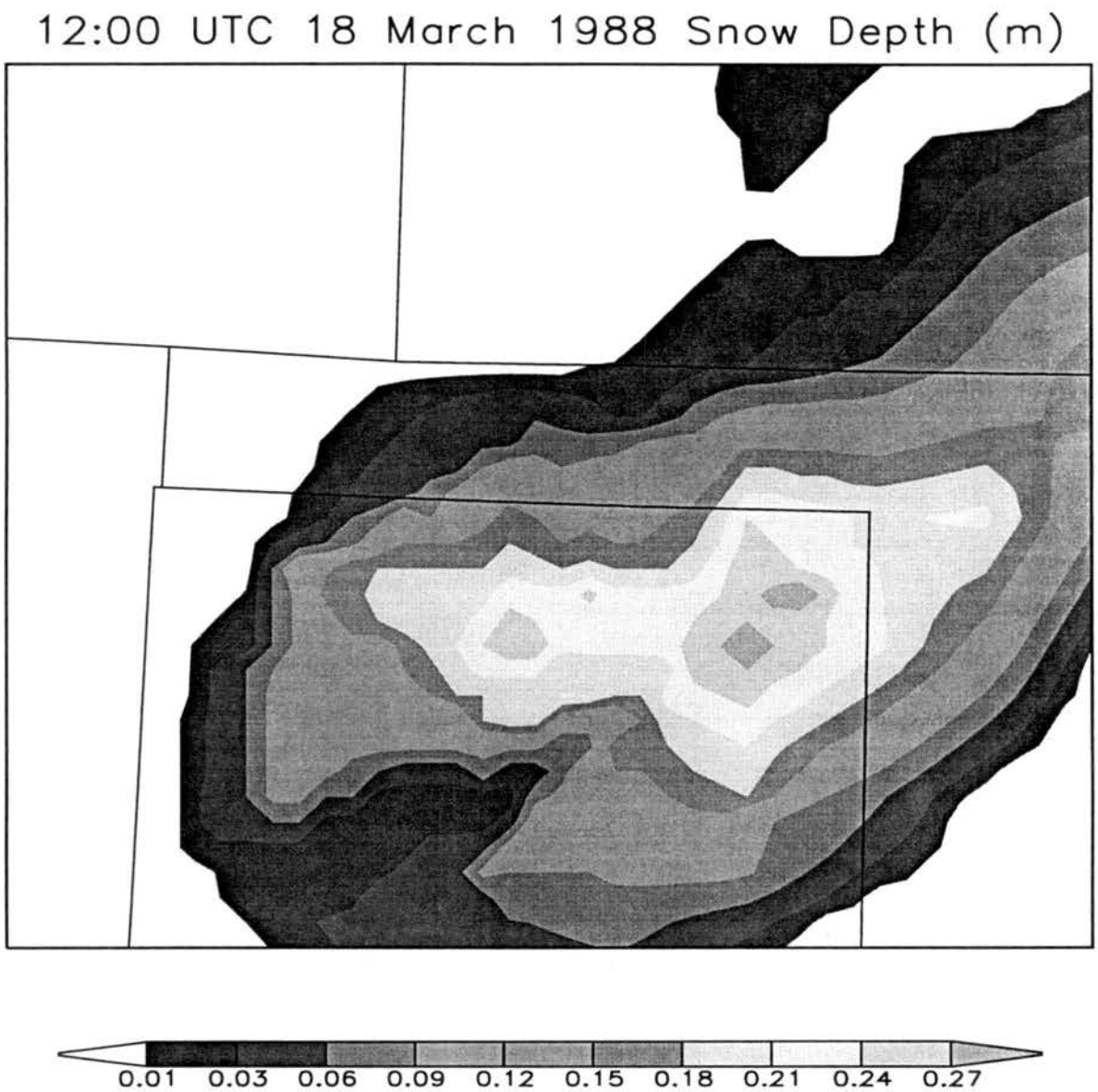

Figure 3.4: Snow depth in meters on model grid at initialization time.

and winds relatively light in the area during the night time hours leading up to the model start time, which is about an hour before local sunrise, the snow temperature is assigned a temperature equal to 3 K less than the lowest model-level (~5 m) air temperature. Under such conditions one would expect significant radiational cooling to lower the temperature of the surface to below that of the low-level air. The internal energy of the snow is then initialized from Equation 2.2.

3.4 Soil Initialization

There are 10 soil layers extending down to 1 m depth. The soil layer thickness ranges from 5 cm near the surface to 20 cm at the deepest level. Soil type is defined as sandy clay loam in all grid cells and at all levels. The methods for assigning initial values of temperature and moisture to the soil are described below.

3.4.1 Soil Temperature

Unfortunately there are no observations of soil temperature for the Texas Panhandle on this date so the temperatures are estimated from the initial screen-height temperature and snow depth. In order to initialize the soil temperature two cases are considered snow covered and snow free. This is done to reflect the insulating effects of snow on the underlying soil. The approach is to first define a snow-free profile and then to warm this slightly according to snow depth.

Soil temperature records have been kept at the Bushland, TX USDA Soil Climate Analysis Network (SCAN) site, located just to the west of Amarillo, since the mid 1990s. These observations are used to estimate the soil temperature profile in the model. First, an average 2 m screen-height temperature of –7°C is determined for the snow-free area in the fine grid. The procedure is then to find March days in the short record at Bushland that have 12 UTC screen-height temperatures within 1°C of –7°C. The days that likely had snow on the ground were excluded. Since Bushland does not record snow depth days with snow were determined based on observations at Amarillo close by to the east. Four acceptable snow-free March days were available from the 5 years of hourly data available at Bushland. In order to determine the most representative of these the weather

Table 3.2: The snow-free temperature profile expressed as an offset from lowest model-level air temperature.

Soil Layer	1	2	3	4	5
Depth (cm)	2.5	7.5	15	25	35
Offset (C)	3.75	9.75	10.5	11.25	11.75
Soil Layer	6	7	8	9	10
Depth (cm)	45	55	65	75	90
Offset (C)	12.25	12.75	13.25	13.75	14.25

for the previous 2 days was compared with that observed for the 2 days leading up to the model simulation. Only the period March 12-14, 1999 had weather that reasonably matched that observed from March 16-18, 1988. The top 40 cm of soil is assumed most sensitive to daily variations in air temperature as suggested in Kuo (1968). Temperatures at progressively deeper levels are less dependent upon daily changes in temperature and correlated more closely with seasonal temperature changes. Even though soil temperature is measured down to 1 m at Bushland only the levels down to 50 cm are used in defining the profile from air temperature for the model. Since in most cases the temperature is observed to continue increasing with depth below 50 cm the model profile is allowed to increase gradually from the 50 cm value to 14.5°C warmer than the lowest model-level ($\sim$5 m) air temperature at the deepest soil layer of 1 m. The temperature of the soil below 40 cm was varied by as much as 10°C and there were no significant impacts on snowmelt or air temperature because of the short duration of the run. The surface is assigned a temperature of 2°C cooler than the lowest model-level air temperature because of radiational cooling. The snow-free temperature profile, expressed as an offset from lowest model-level air temperature, is shown in Table 3.2. The depths represent the mid-points of the 10 soil layers. The lowest model-level temperature is assumed 1°C warmer than the screen-height temperature and so the values in Table 3.2 are derived by subtracting 1°C from offsets from the screen-height temperature calculated from the Bushland profile.

A rough estimate of the insulating effect of snow is obtained from some daily measurements taken in the former USSR between 1941 and 1948 listed in Shul'gin (1957).

This data suggests that for 10 cm deep snow the 3 cm soil depth temperature is about 2°C warmer than when the soil is snow free when the minimum air temperature is –10°C. The influence of the snow on soil temperature will decrease with soil depth and it is assumed that the difference between snow-covered and snow-free soil temperatures decreases linearly to 0 at 30 cm. To get the temperature difference at the soil surface this profile is simply extrapolated linearly to the surface; see Figure 3.5. The influence of the snow on soil temperature will also decrease with decreasing snow depth. This effect is also modeled in a simple linear fashion so that the snow-covered/snow-free difference in the soil surface temperature decreases linearly from its value when snow depth is 10 cm to 0 when snow depth is 0; see Figure 3.5. With some algebra we can now derive a simple equation, shown below, for the insulating strength of snow, ΔT_z, as a function of snow depth, z_s, and soil depth, z_g.

$$\Delta T_z = 74.07 z_s (0.3 - z_g) \tag{3.1}$$

The ΔT_z values for each level are then added to the bare soil temperature offset profile, listed in Table 3.2, to produce the snow-covered soil temperature profile.

If the initial temperature for any soil layer, as determined from the above profile, is below the freezing point then a further correction is made to account for the latent heat of fusion given off when the moisture in the layer freezes. As the top surface of the soil begins to freeze its temperature will remain at 0°C until all of the moisture is frozen. In order to account for this a comparison is made between the energy loss ($Q1$) required to cool the soil and its moisture, in liquid form, to the subfreezing temperature predicted by the above profile and the amount of energy ($Q2$) which must be released to freeze all the moisture in the soil layer. If $Q1$ is less than $Q2$ then the soil temperature is set to 0°C and an ice fraction is computed using Eq. 2.1 with $Q_g = Q2 - Q1$. If $Q1$ is greater than $Q2$ then the ice fraction is set to 1 and the soil temperature is computed from Eq. 2.1 with $Q_g = Q2 - Q1$. This procedure assigns a temperature of 0°C, with the moisture partly in the form of ice, to the top 5 cm soil layer over most of the snow-free areas of the fine domain.

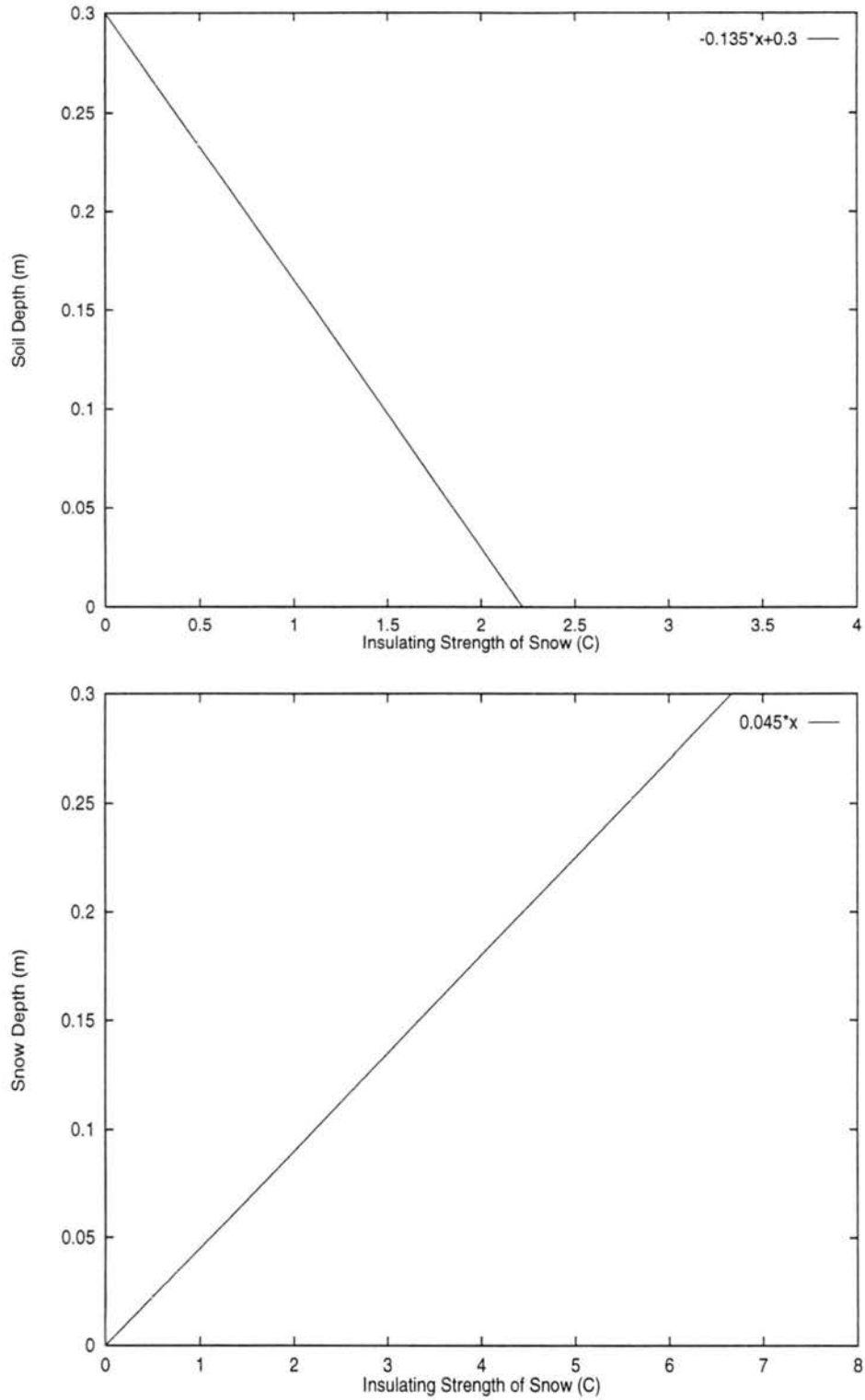

Figure 3.5: Top panel: Variation of the insulating strength of the snow with soil depth, expressed in degrees C. Bottom panel: Variation of the insulating strength of the snow at the soil surface as a function of snow depth, expressed in degrees C.

3.4.2 Soil Moisture

The soil moisture is initialized with output from a single layer soil model described in Huang et al. (1996). The model uses observed monthly temperature and precipitation data for the 344 U.S. Climate divisions to estimate runoff, evaporation, and soil moisture. Data is available from the Climate Prediction Center for the last day of each month from 1931 to the present. The values for March 18, 1988 are linearly interpolated from the output for February 29 and March 31 1988.

Chapter 4

RESULTS

4.1 Control Run

In this chapter a discussion of the results of the control run is given. Observed screen-height air temperatures and potential temperature profiles at Amarillo, TX and Dodge City, KS; see Figure 4.1, are compared with the control run output. Amarillo had 5 cm of snow on the ground at initialization time and Dodge City was snow free during the entire simulation. The comparisons with these two sites will give some insight into how well the model can simulate air temperature and boundary-layer evolution over both snow-covered and snow-free ground.

Since the evolution of air temperature and boundary-layer structure are controlled by the surface sensible and latent heat fluxes it is also important that they be checked against observations. Observations of sensible and latent heat fluxes along the SSBLIM flight path shown in Figure 4.1 are compared to those generated by the model. Potential temperature and surface albedo measured along this flight path are also compared with the model output.

4.1.1 Potential Temperature Profiles and Screen-Height Air Temperature

The potential temperature profiles for 12 UTC 18 March 1988 (model start time) and 00 UTC 19 March 1988 at Amarillo, TX are shown in Figure 4.2. At the start of the simulation Amarillo had 5 cm of snow on the ground. The initial profiles in the model are the result of interpolation of the reanalysis and upper air observations to the RAMS grid. The model profiles that are compared with observed soundings in the following discussion are taken at the model grid point located nearest the station where the observations were made. Since the horizontal grid increments are 10 km the model profile does not coincide

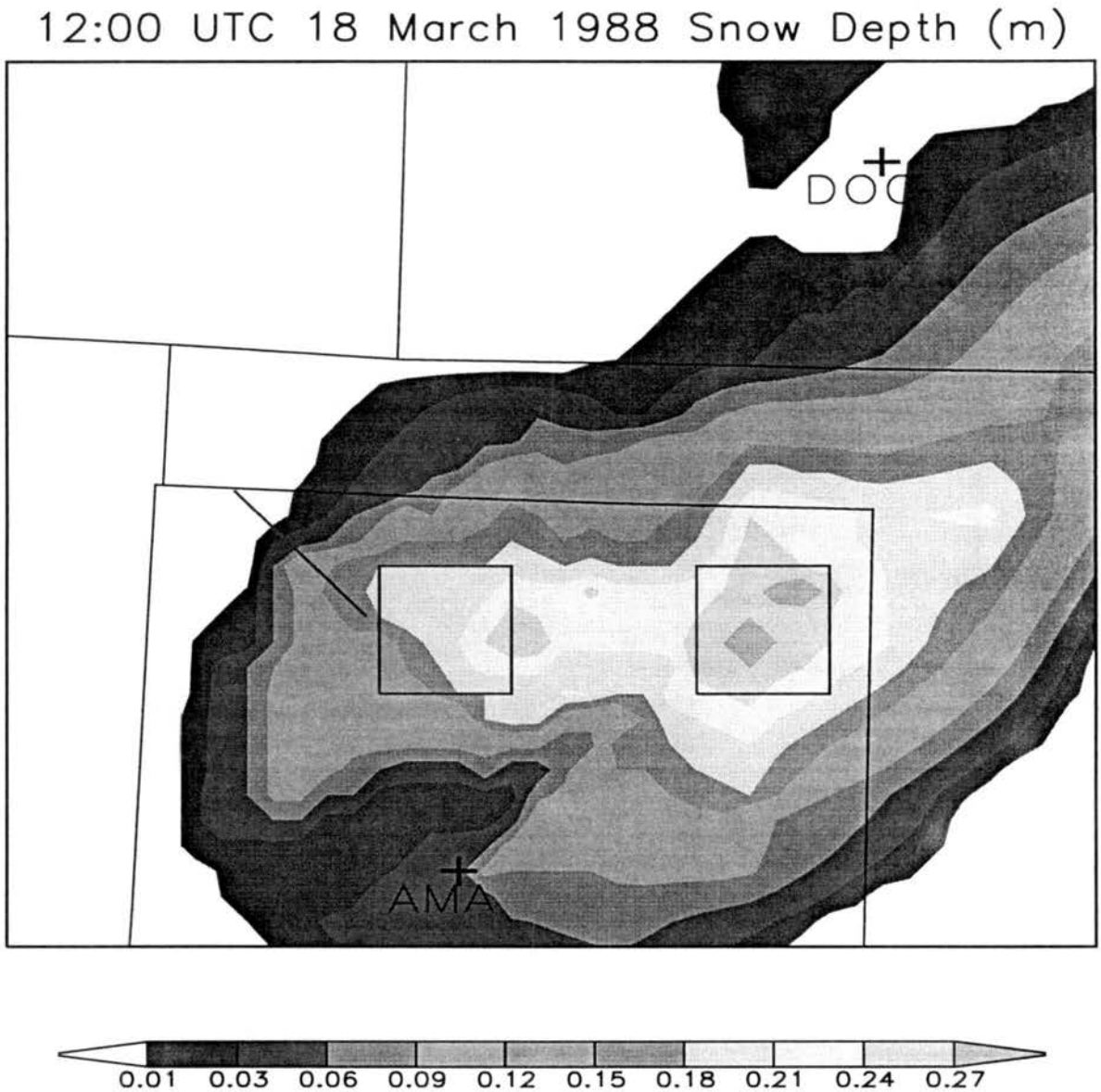

Figure 4.1: Snow depth in meters at model initialization time (12 UTC 18 March 1988). Locations of Amarillo, TX and Dodge City, KS are shown by crosses marked AMA and DOC respectively. The red line shows location of SSBLIM flight track. The left red box shows the location of region 1 and the right red box shows location of region 2.

exactly with the location of the station. For this reason the initial model profiles will not match exactly with the observed soundings. Looking at Figure 4.2 we can see that the model has simulated the evolution of the potential temperature profile well in the lowest 2000 m. At the end of the 12 hour simulation the model-generated potential temperature is within 1 K of the observations. The largest errors occur in the lowest 600 m. This could be due to the cool bias at the lowest levels in the initial model profile. Since the initial sounding is too cool in the lower levels it would not be unreasonable to expect the afternoon profile to be too cool near the surface.

Potential temperature profiles at Dodge City, KS for the same times are also shown in Figure 4.2. Dodge City was snow free during the entire simulation. The model potential temperature is generally within 2 K. In this case the model profile is too warm at all levels below 2000 m. By 00 UTC significant warming, $\sim$8 K, has occurred above the base of the inversion in both the model and observed profiles. This is likely the result of subsidence under a high pressure system located over the region. Subsidence ranging from 2 to 6 cm s^{-1} occurs in the model over the region during the entire simulation. Looking at the initial model profile we see that it is 1-2 K too cool in the 200-600 m height range. However, the model profile is also less stable than the observed profile. This means the model profile will become unstable more quickly allowing it to warm to greater depths by afternoon. Although the results are not perfect it should be taken into consideration that some of the larger errors could be explained by errors in the initial profiles due to interpolation as explained earlier.

Figure 4.3 shows a time series of the screen-height temperature at both Amarillo and Dodge City. The simulated temperatures are never more than 2°C from observations and usually within 1°C. This provides evidence of the ability of RAMS 4.30 to reasonably simulate the evolution of low-level temperature over snowy and snow-free areas.

4.1.2 Comparison with SSBLIM Observations

Figure 4.4 shows sensible and latent heat fluxes as measured by the eddy covariance technique as descried in Appendix D of Cramer (1988), along the 90 m altitude flight track shown in Figure 4.1. The dark bar at the bottom of each panel represents the part of the

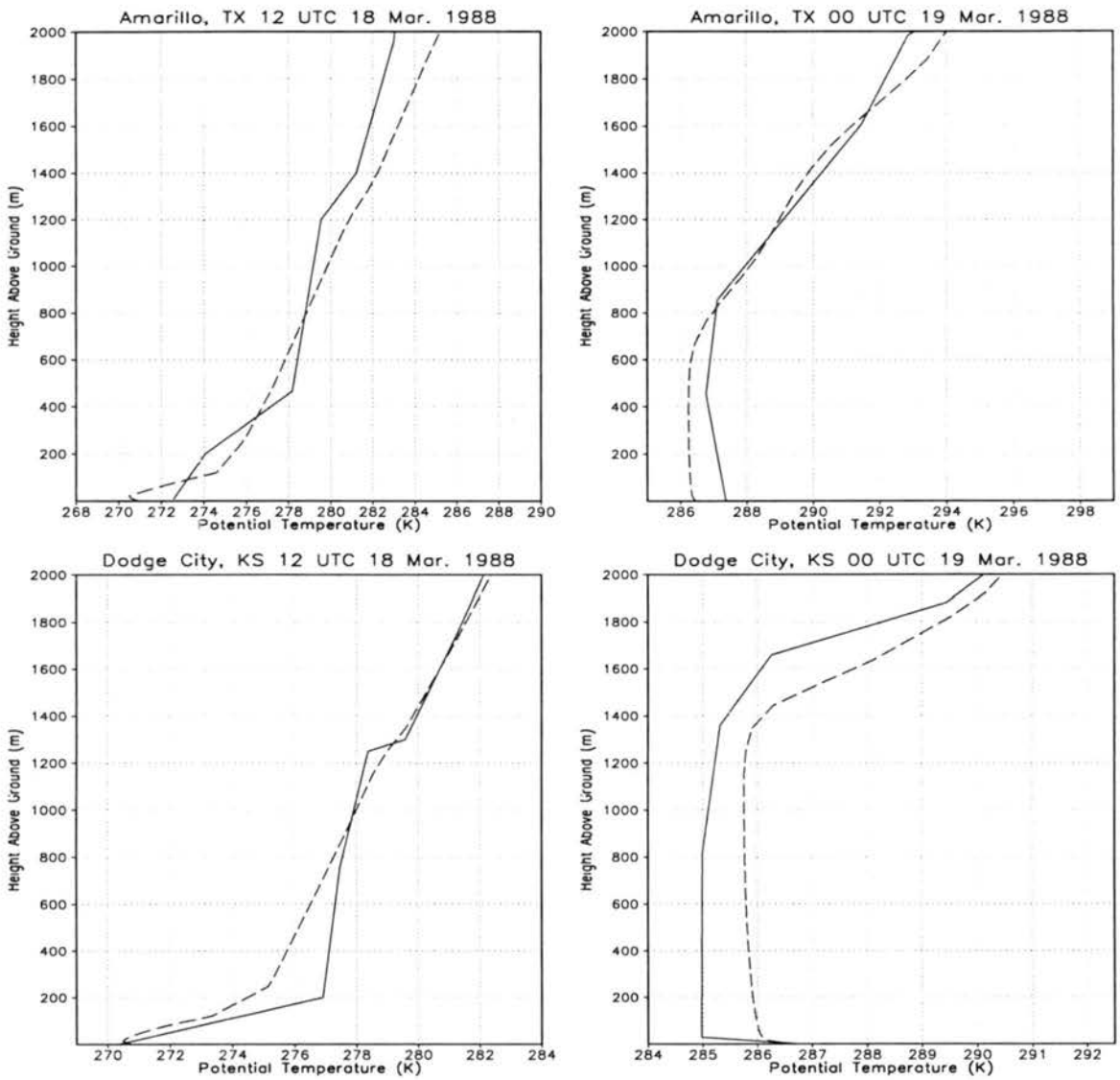

Figure 4.2: Comparison of control run potential temperature profiles with observations. Solid and dashed lines represent the observed and model simulated profiles respectively.

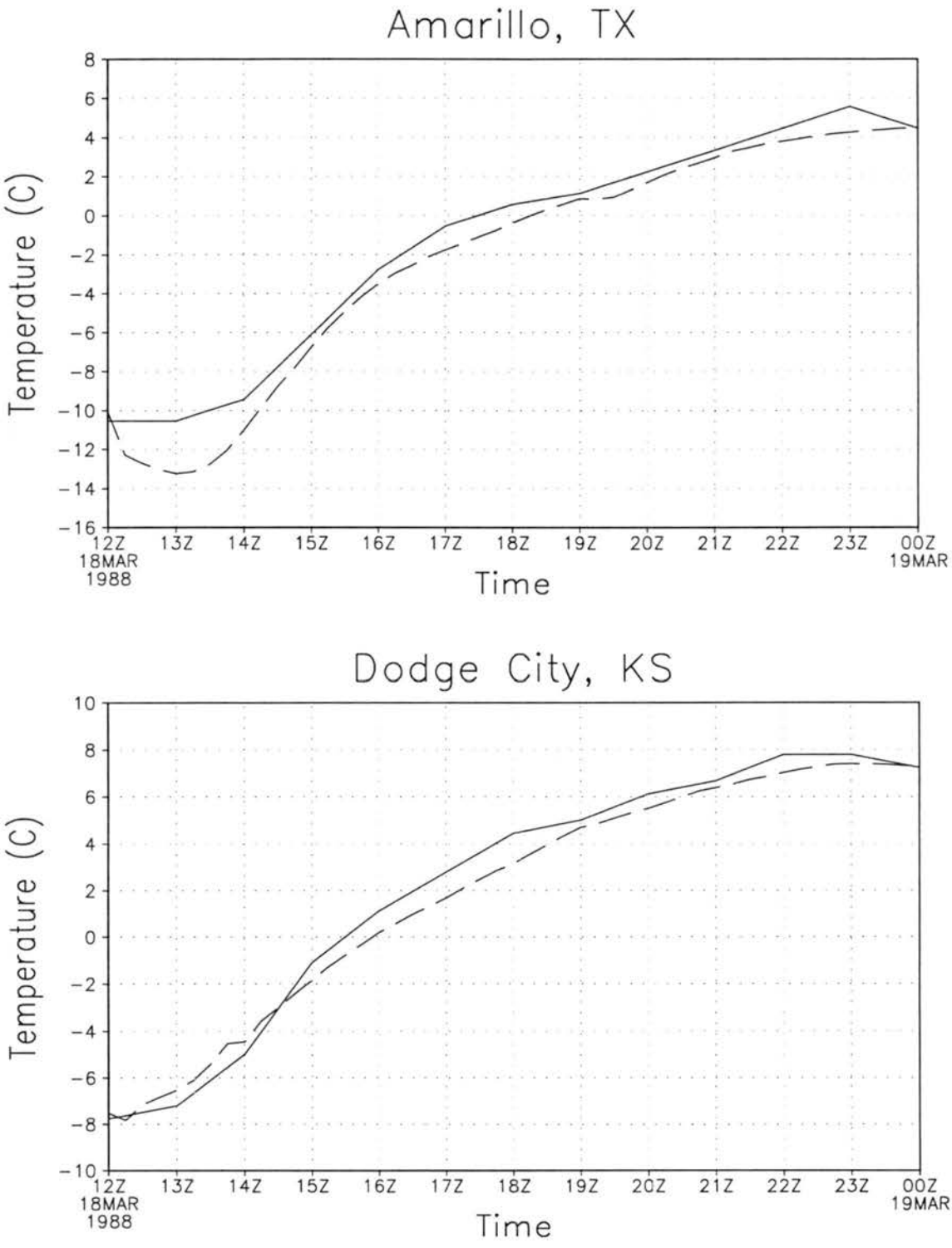

Figure 4.3: Comparison of control run screen-height temperatures with observations. Solid and dashed lines represent the observed and simulated temperatures respectively.

flight track that was over snow. Two 90 m altitude flights were made over the snow on the afternoon of 18 March 1988. During the first flight the sensible heat fluxes ranged from 210 W m^{-2} over the snow-free areas to 20 W m^{-2} over the snow-covered regions. From Figure 4.4 it can be seen that the simulated sensible heat fluxes at 90 m are mostly within 40 W m^{-2} of the observed values. The largest errors, around 80 W m^{-2}, are near the snow/no-snow boundary. It could be that the model is underestimating the sensible heat flux here due to its inability to resolve the possible fine-scale patchiness of the melting snow cover in this area.

In Figure 4.4 we can see that the observed latent heat flux is highest over the snow/no-snow boundary. The smallest values of ~20 W m^{-2} are observed over the snow-free area, with slightly higher values, around 30-40 W m^{-2}, over the snow-covered area. The maximum over the snow/no-snow boundary region may be due to warmer and drier air from the snow-free region being advected over the melting snow by the northwesterly winds. The model correctly simulates the maximum over the snow/no-snow boundary and minimum over the snow-free areas. The model is generally within 10-20 W m^{-2} of the observed values. The worst errors occur over the snow where the model underestimates the fluxes by as much as 40 W m^{-2}.

Figure 4.5 shows that the observed sensible heat flux along the second flight ranges from 150 W m^{-2} over the snow-free portion of the track to 20 W m^{-2} over the snow. As in the first case the simulated values are often within 40 W m^{-2} of the observed values. The model is again too low over the snow/no-snow boundary. In this case there is also a large error, 60 W m^{-2}, over part of the snow-free area. Figure 4.5 shows that the observed latent heat flux in the second flight has the same general pattern as in the first flight. The simulated values are generally within 10 W m^{-2} of the observed values.

Comparisons of flight-level potential temperature and surface albedo for the first flight are shown in Figure 4.6. From the top panel of Figure 4.6 it can be seen that the observed potential temperature ranges from as high as 290 K over the snow-free areas to as low as 284 K over the snow. The simulated values at 90 m are generally within 1 K of the observed values. The largest errors are once again over the snow/snow-free boundary region. In this

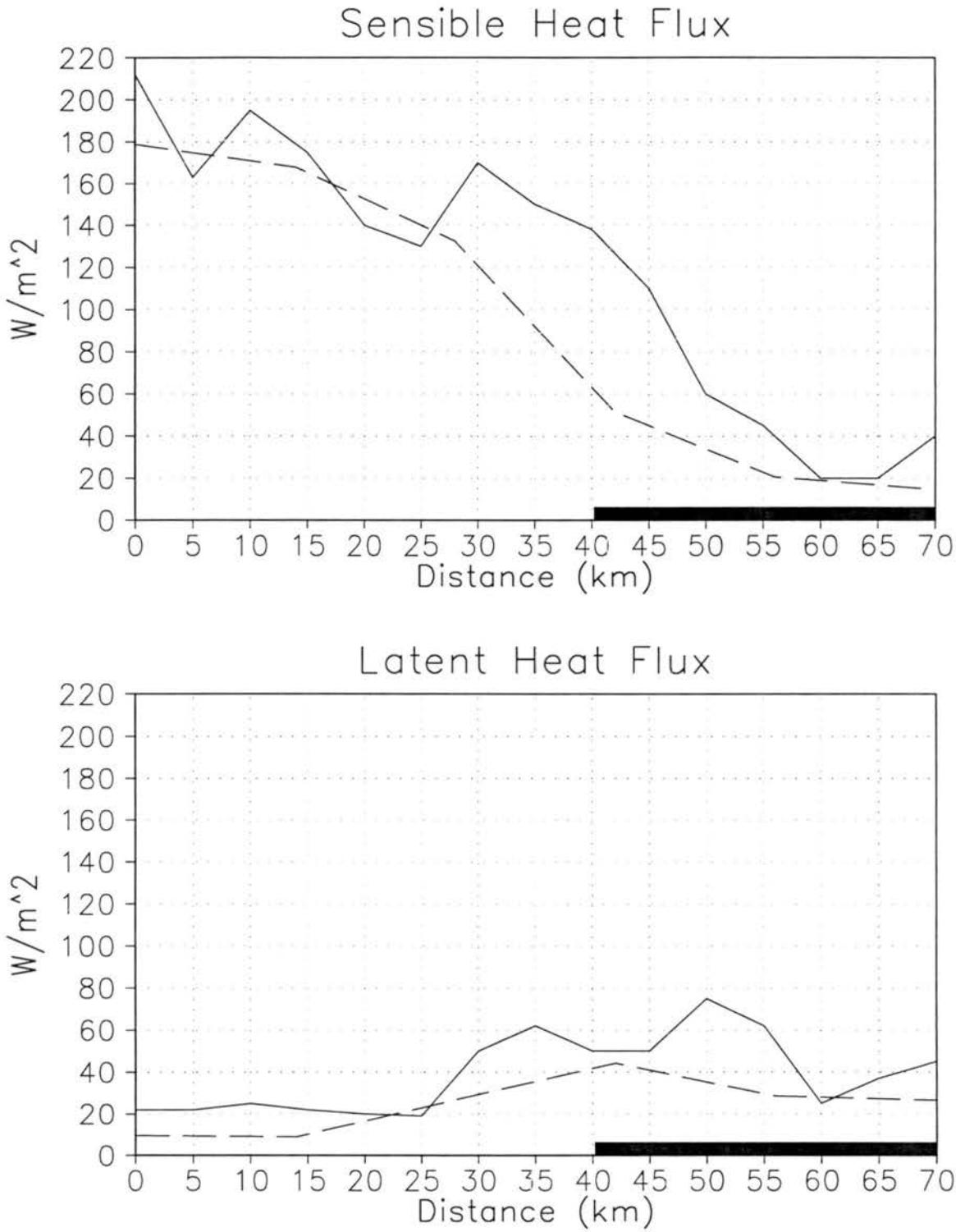

Figure 4.4: Sensible and latent heat flux along the first (2013 UTC - 2028 UTC) 90 m altitude SSBLIM flight. Solid and dashed lines represent the SSBLIM and control run generated values respectively. The bar along the distance axis of each panel shows the portion of the flight over snow.

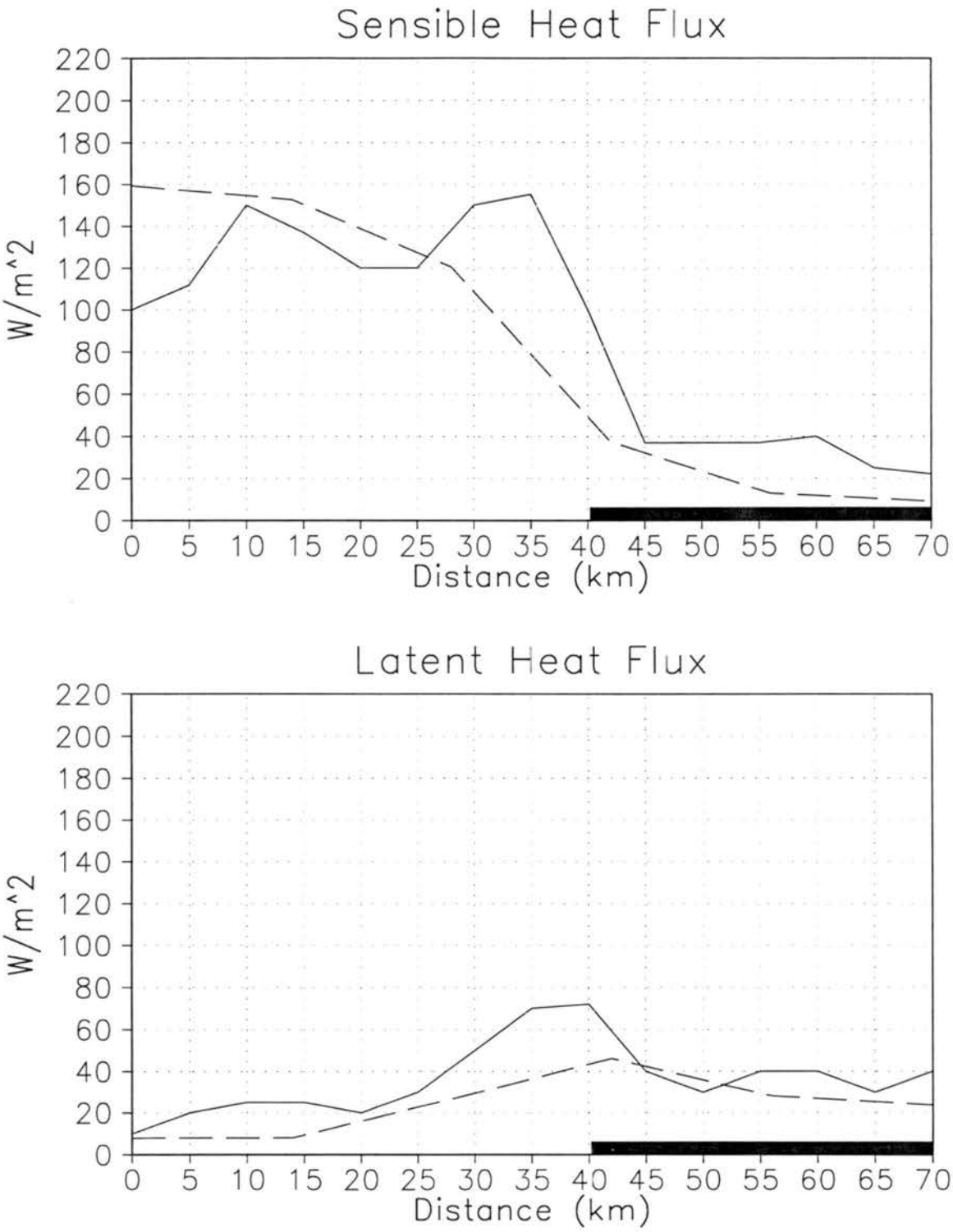

Figure 4.5: Same as in Figure 4.4 except for second SSBLIM flight (2121 UTC - 2136 UTC).

region the simulated temperatures are too cool, likely due to the underpredicted sensible heat flux there. The bottom panel of Figure 4.6 shows that the net surface albedo as measured by the aircraft ranges from a low of around 0.2 over the snow-free areas to as high as 0.65 over the snow. The simulated albedo is also right around 0.2 over the snow-free region. Over the snow-covered region the model albedo reaches a high of about 0.5 which appears to be a bit high on average, but is still a reasonable approximation of the albedo in the snow area. As seen in Figure 4.6, the observed albedo of the snow covered area varies quite rapidly from as low as 0.3 to as high as 0.65, illustrating the likely high degree of surface land-cover heterogeneity in the region. The 10 km grid cells of the model will not be able to resolve such rapid variations in albedo and so an average value is the best that can be done.

Finally, the potential temperature and albedo for the second flight are shown in Figure 4.7. The top panel shows that the potential temperature has warmed along the entire track, which is to be expected since the second flight occurred about an hour later in the afternoon. Again the simulated potential temperature is within about 1 K of the observations along most of the track. The observed surface albedo has decreased some over the snow due to melting. The simulated albedo has decreased slightly over the snow also, but appears once again to be slightly too high on average.

4.2 Simulation 2

In simulation 2 the AVHRR-derived land-cover data has been used with OGE classes 40 and 41, the shrub/grass mixture classes, cross referenced to deciduous shrubs. Everything else has remained the same as in the control run. The differences between this run and the control will be examined over two regions, shown by the squares in Figure 4.1, of the fine domain. Each of the regions are 50 km by 50 km. The western region, which will be called region 1, is located over an area consisting predominately of crop land and short grass according to the Landsat data; see Figure 4.8. The eastern region, which will be called region 2, consists of mostly short grass with a few areas of shrubs and crop land; see Figure 4.9. Figures 4.10 and 4.11 show the fractional land-cover breakdown for the two

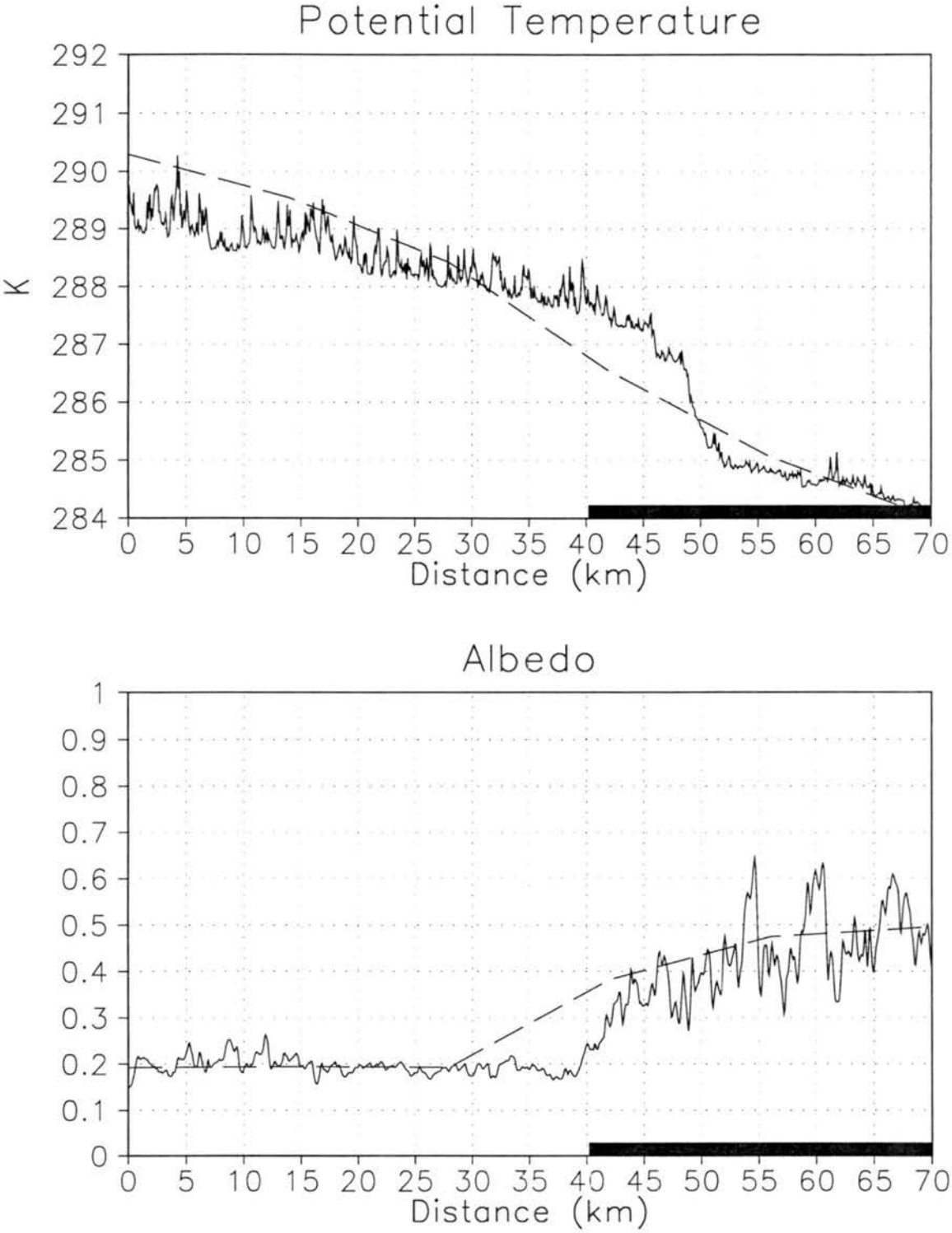

Figure 4.6: Potential temperature and surface albedo along the first SSBLIM flight (2013 UTC - 2028 UTC). Solid and dashed lines represent the SSBLIM and control run generated values respectively. The bar along the distance axis of each panel shows the portion of the flight over snow.

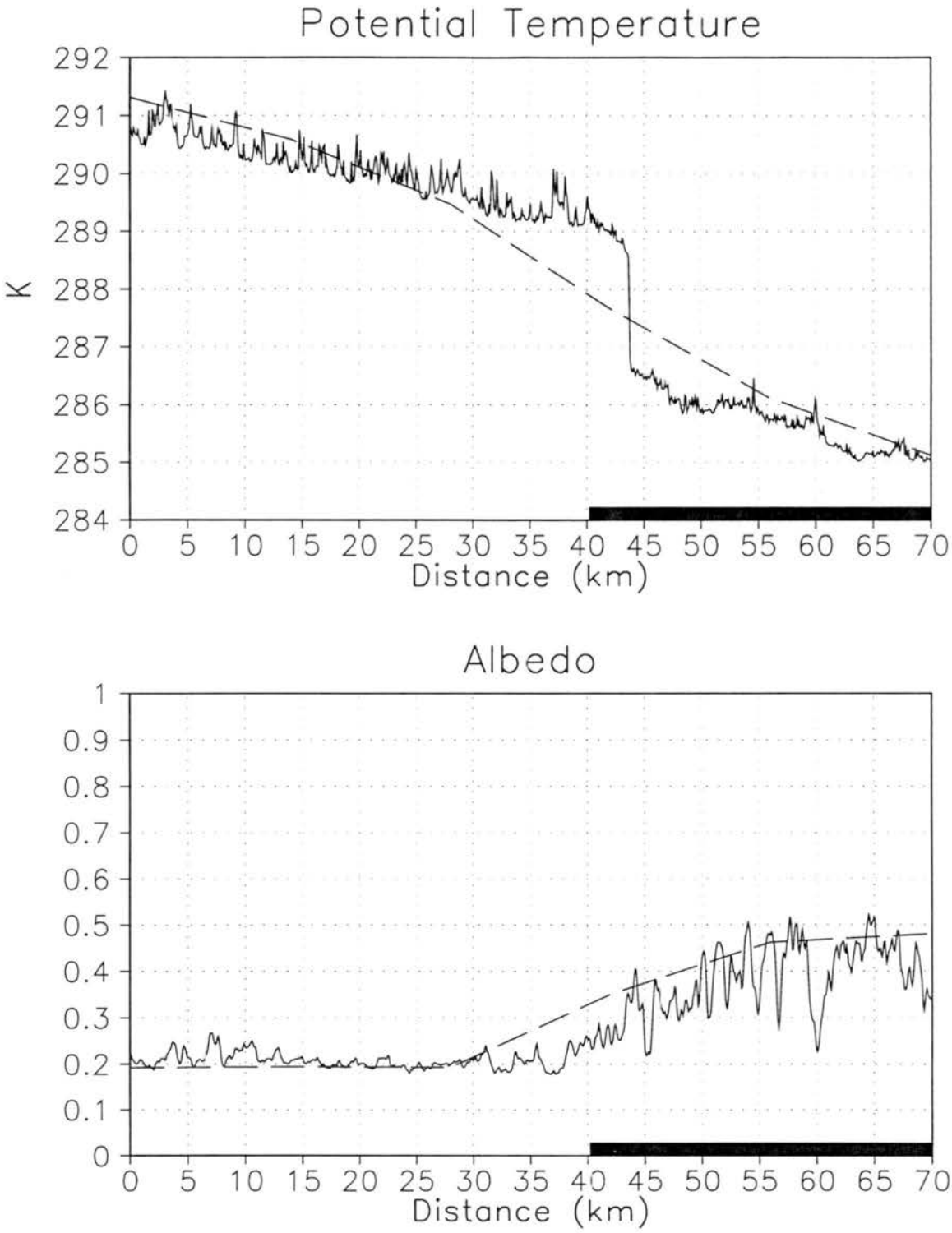

Figure 4.7: Same as in Figure 4.6 except for second SSBLIM flight (2121 UTC - 2136 UTC).

regions as defined from the AVHRR data used in simulation 2. From Figure 4.10 it can be seen that region 1 is now mostly shrubs, with virtually no short grass. The crop areas, defined as crop stubble or winter wheat, are also significantly less. A look at Figure 4.11 shows that region 2 is now mostly shrubs instead of short grass and the crop areas have increased slightly. The effects of these land cover changes on surface sensible and latent heat fluxes, air temperature, snowmelt, and boundary-layer structure in the two regions are discussed below.

4.2.1 Region 1

In this case the switch from Landsat to AVHRR land-cover data and the choice of cross referencing the shrub/grass mixture to all shrubs has significantly reduced the crop and short grass areas as shown in Figures 4.8 and 4.10. The average snow depth in region 1 at model initialization time is about 0.19 m. Referring back to Table 3.1 it can be seen that the crop areas will be completely masked by snow of this depth, while the short grass will be partially masked, and the shrubs mostly exposed. Since in this case the shrub fraction has increased at the expense of short grass and crops it is expected that higher sensible heat fluxes will occur in simulation 2 than in the control run. The taller protruding shrubs will emit most of the solar energy they absorb in the form of upward turbulent sensible heat flux.

A look at Figure 4.12 shows that this is indeed the case. The top panel shows the evolution of the area-averaged surface sensible heat flux from region 1. The surface sensible heat fluxes for the control run and simulation 2 both increase from negative values around sunrise to maximum positive values in the early afternoon and then decrease to near zero by early evening. However, the morning increase is much more rapid in simulation 2, shown by the dashed line, and sensible heat flux is some 60-80 W m^{-2} greater than in the control simulation, shown by the solid line, for much of the day. This is what is expected since the tall shrubs protrude through the snow in simulation 2 allowing for more solar radiation to be absorbed during the course of the day. The sensible heat flux in simulation 2 peaks and begins to decrease earlier in the afternoon than in the control run since the sparse shrubs have a lower heat capacity than the snow.

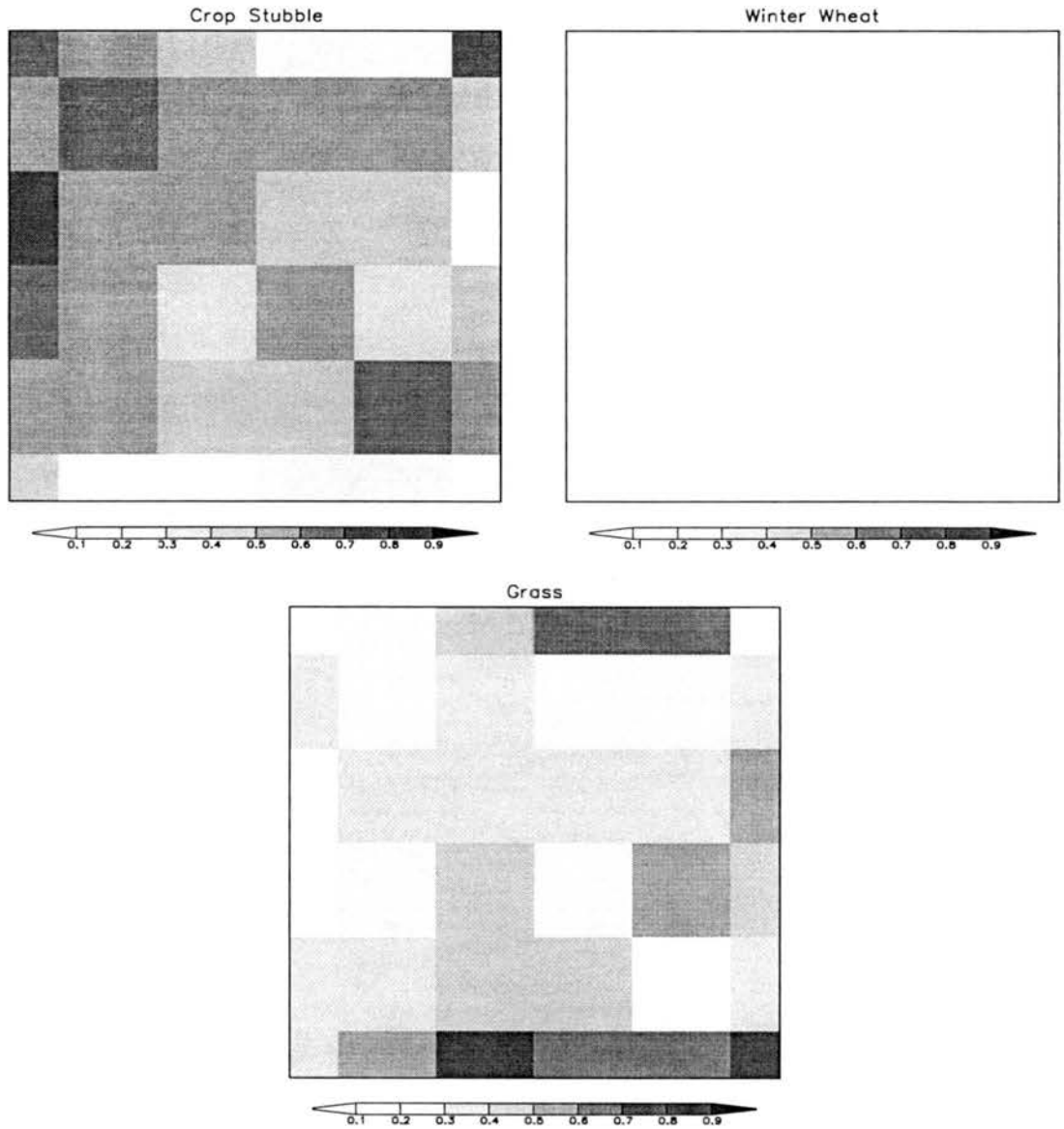

Figure 4.8: Fraction of each grid cell in region 1 that is occupied by the major land-cover categories as determined from the Landsat data.

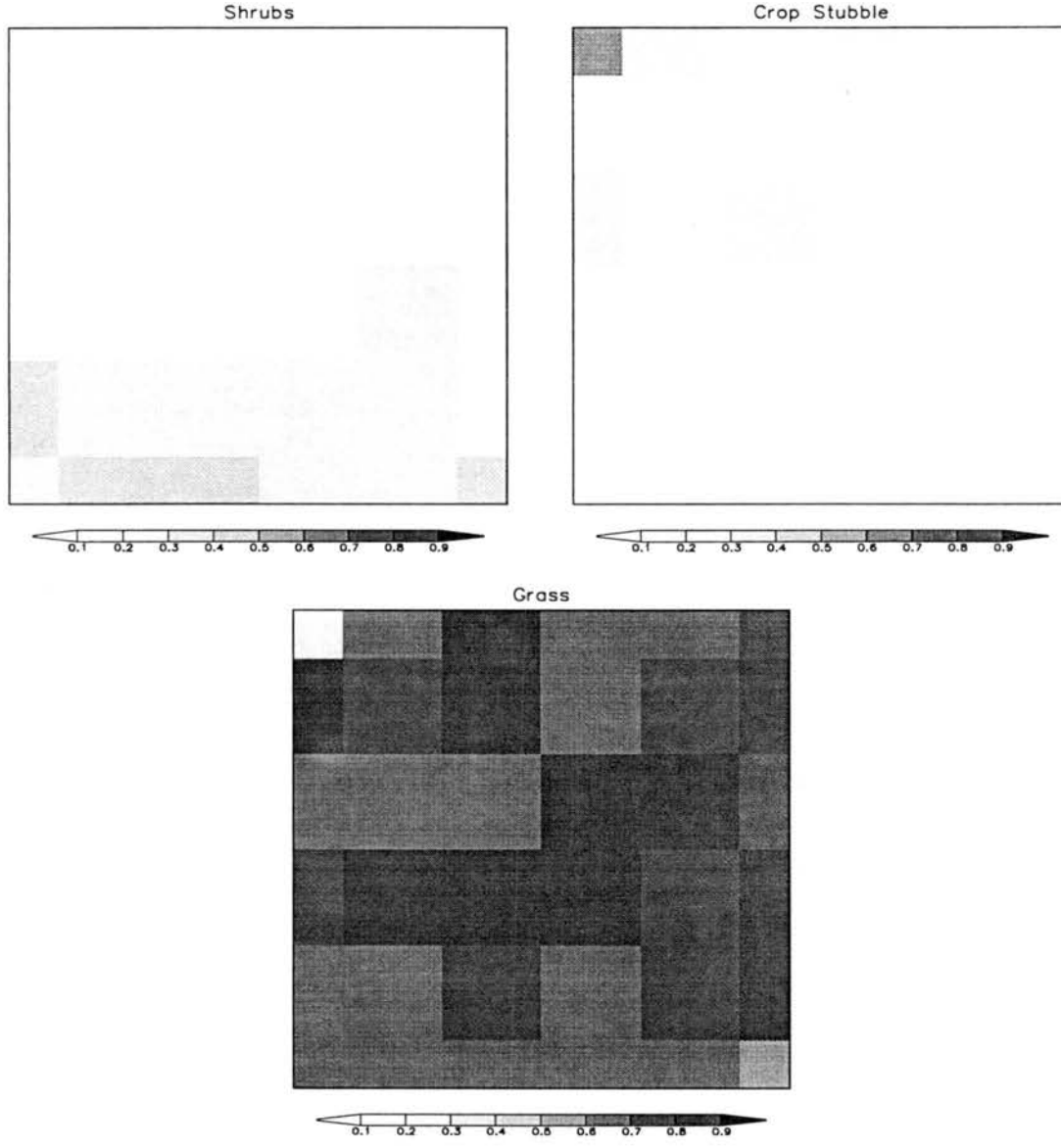

Figure 4.9: Same as for Figure 4.8 except for region 2.

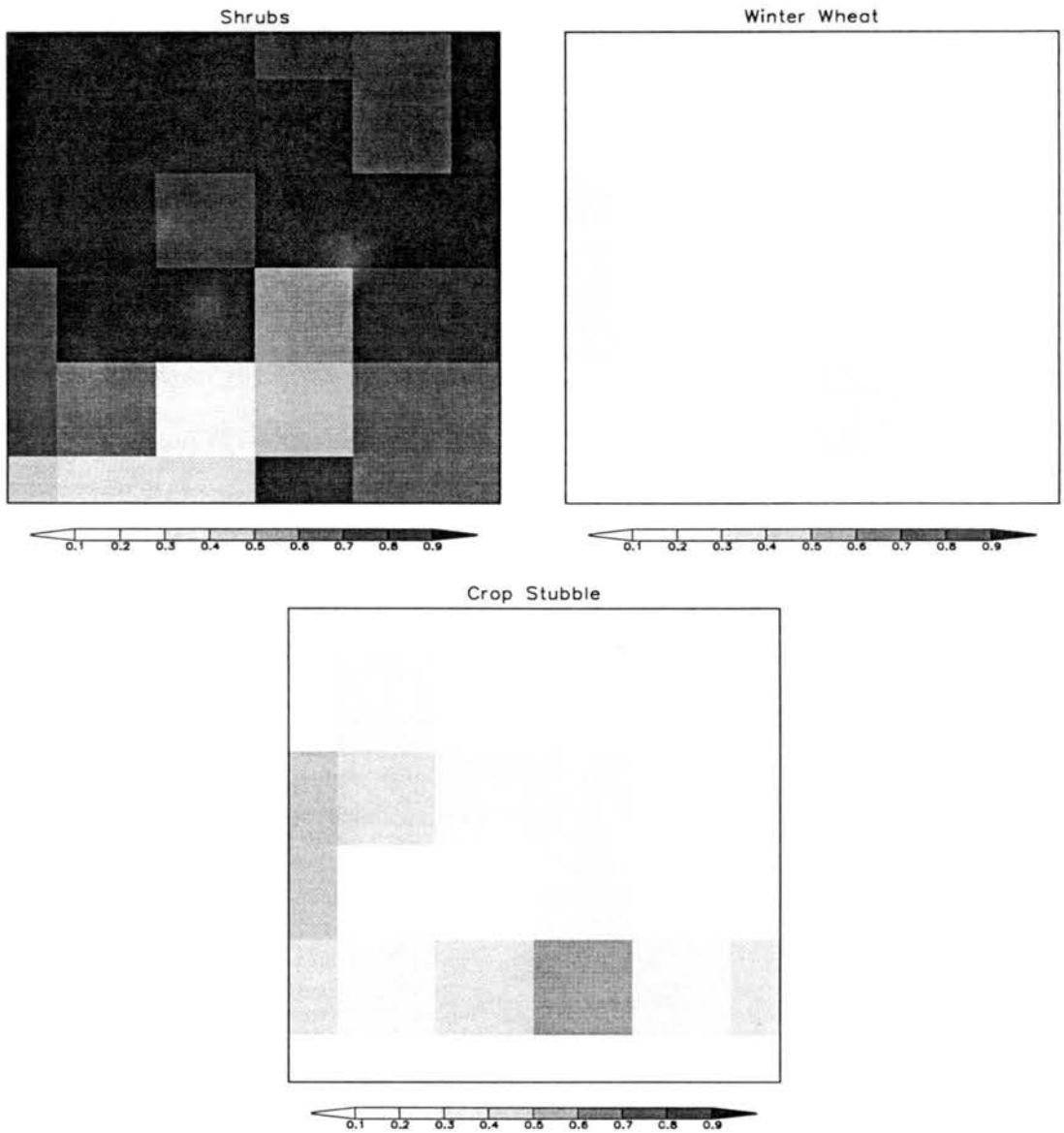

Figure 4.10: Fraction of each grid cell in region 1 that is occupied by the major land-cover categories as determined from the AVHRR data with the shrub/grass mixture defined as all shrubs.

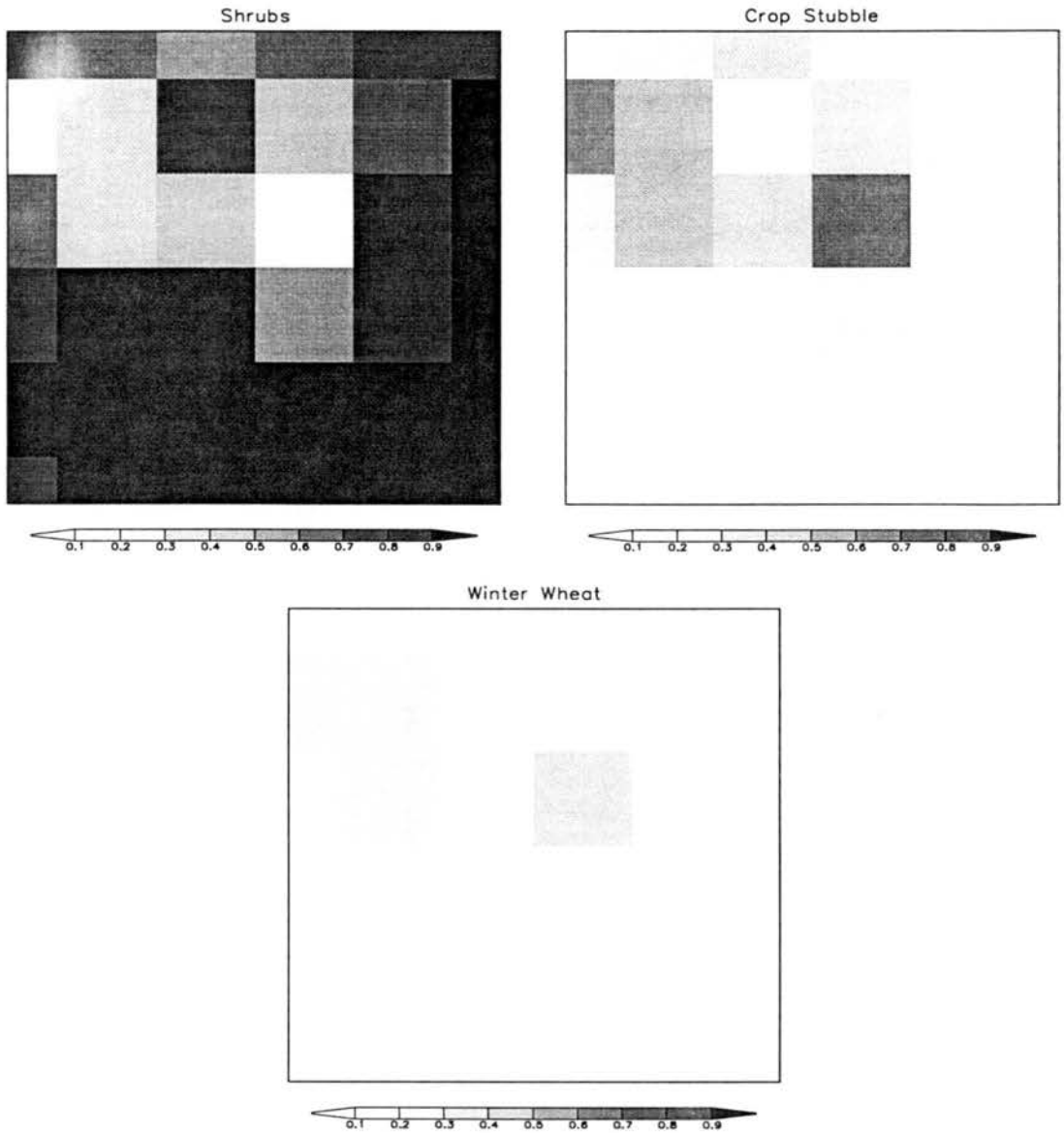

Figure 4.11: Same as Figure 4.10 except for region 2.

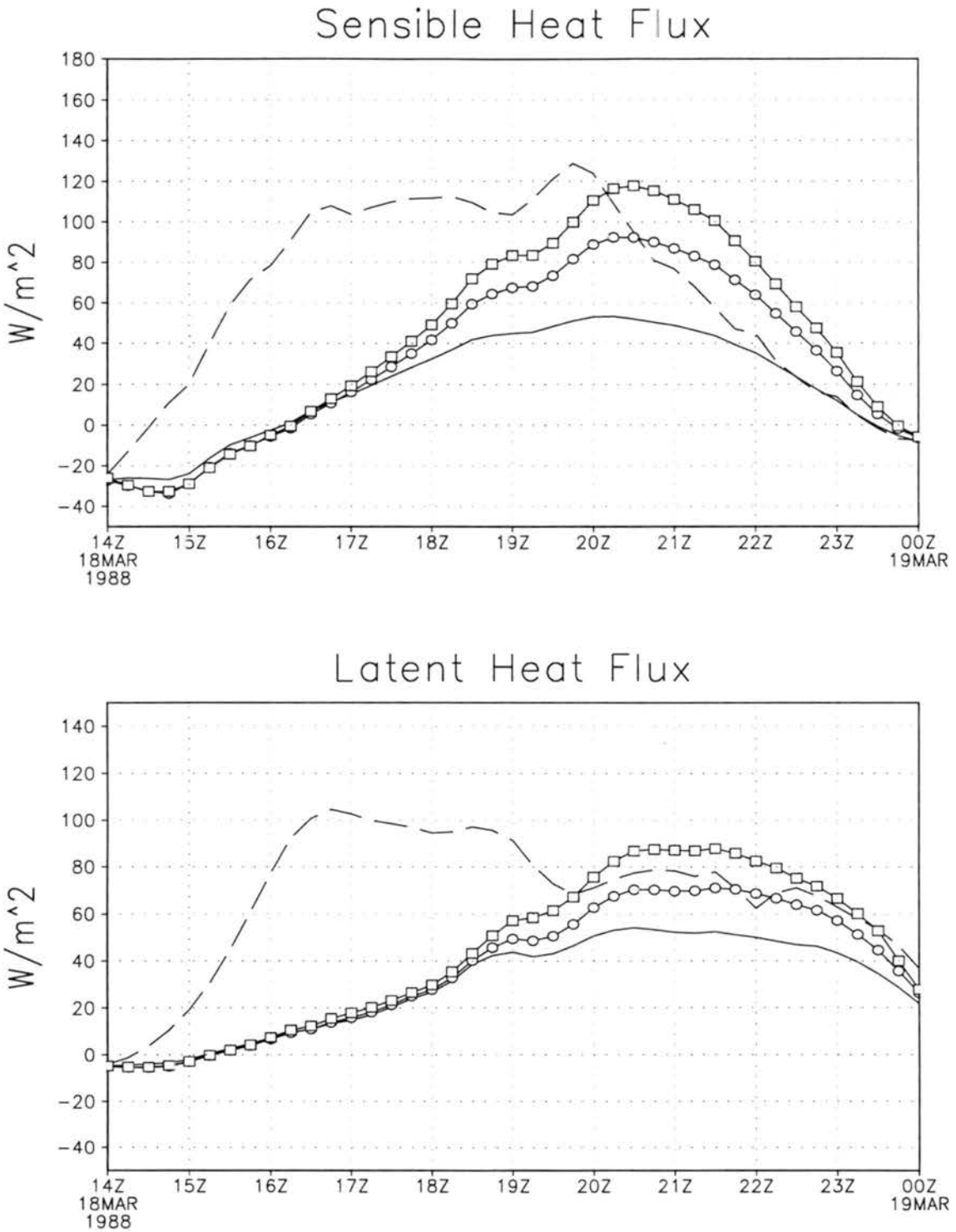

Figure 4.12: Area-averaged sensible and latent heat fluxes over region 1. Solid line is for control run, dashed line for simulation 2, line with circles is for simulation 3, and line with squares is for simulation 4.

The bottom panel of Figure 4.12 shows the evolution of the area-averaged latent heat flux over the course of the day. The latent heat flux in this case will be due almost solely to evaporation of moisture from the snow and soil surfaces. Transpiration is virtually non-existent because the vegetation is either dead or senescent. As shown in Figure 4.12 the latent heat flux increases much more rapidly in simulation 2 than in the control run during the morning. This is likely a result of the higher surface sensible heat flux increasing the turbulent transfer. The latent heat flux begins to decrease in the early afternoon, around 19 UTC, because in some areas the snow has already completely melted meaning the supply of moisture for evaporation has been reduced. The small spike in sensible heat flux right after 19 UTC in simulation 2 is also a result of the emergence of snow-free areas. In contrast, in the control simulation the latent heat flux initially increases much more slowly than in simulation 2 and, following the sensible heat flux, peaks later in the afternoon.

The evolution of the area-averaged 5 m air temperature and snow depth is plotted in Figure 4.13. In the top panel it can be seen that the air temperature in simulation 2 is as much as 6°C warmer than in the control run during the mid-morning. This is a direct result of the much greater surface sensible heat flux during this time in simulation 2. The difference in air temperature between the two simulations decreases by mid-day, possibly because of advection of warmer air from the snow-free areas to the northwest by the prevailing northwesterly flow. The bottom panel of Figure 4.13 shows that more of the snow melts in simulation 2. From Figure 4.14 we see that the total amount of longwave, shortwave, and sensible heat energy absorbed by the snow is between 50 and 100 W m^{-2} greater during the course of the day in simulation 2 than in the control simulation. The amount of solar radiation absorbed by the snow in simulation 2 is actually less than in the control run because of the shading effect of the protruding shrubs; see Figure 4.14. However, the increased longwave and sensible heat fluxes from the protruding vegetation in simulation 2 more than offset the reduction in absorbed solar radiation leading to a net increase in the amount of energy absorbed by the snow in simulation 2.

Finally, Figure 4.15 shows that the mid-afternoon boundary layer is about 300 m deeper in simulation 2 than in the control run, another consequence of the increased sensible heat flux. Also, the profile in simulation 2 is about 1 K warmer than the control run

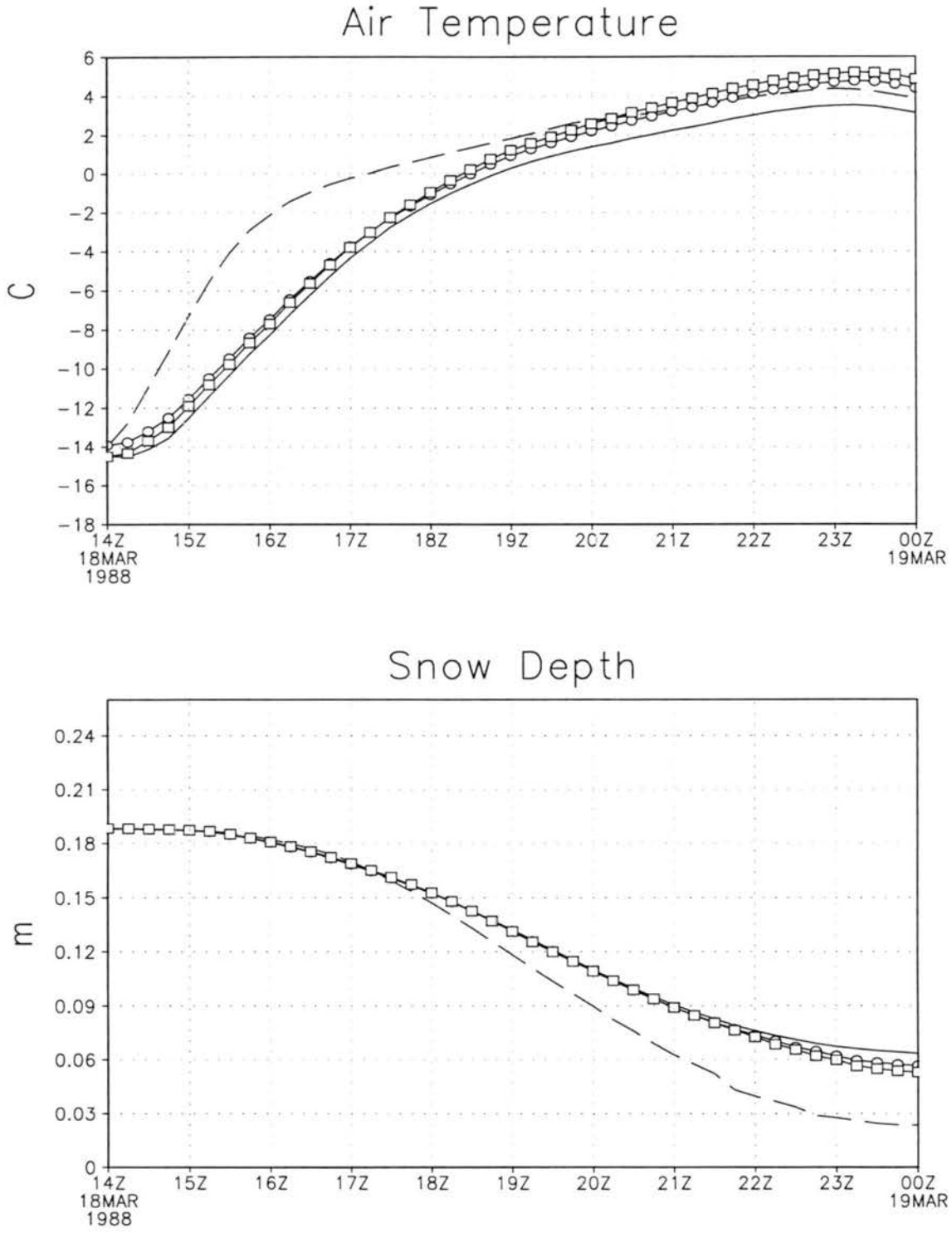

Figure 4.13: Area-averaged 5 m temperature and snow depth over region 1. Solid line is for control run, dashed line for simulation 2, line with circles is for simulation 3, and line with squares is for simulation 4.

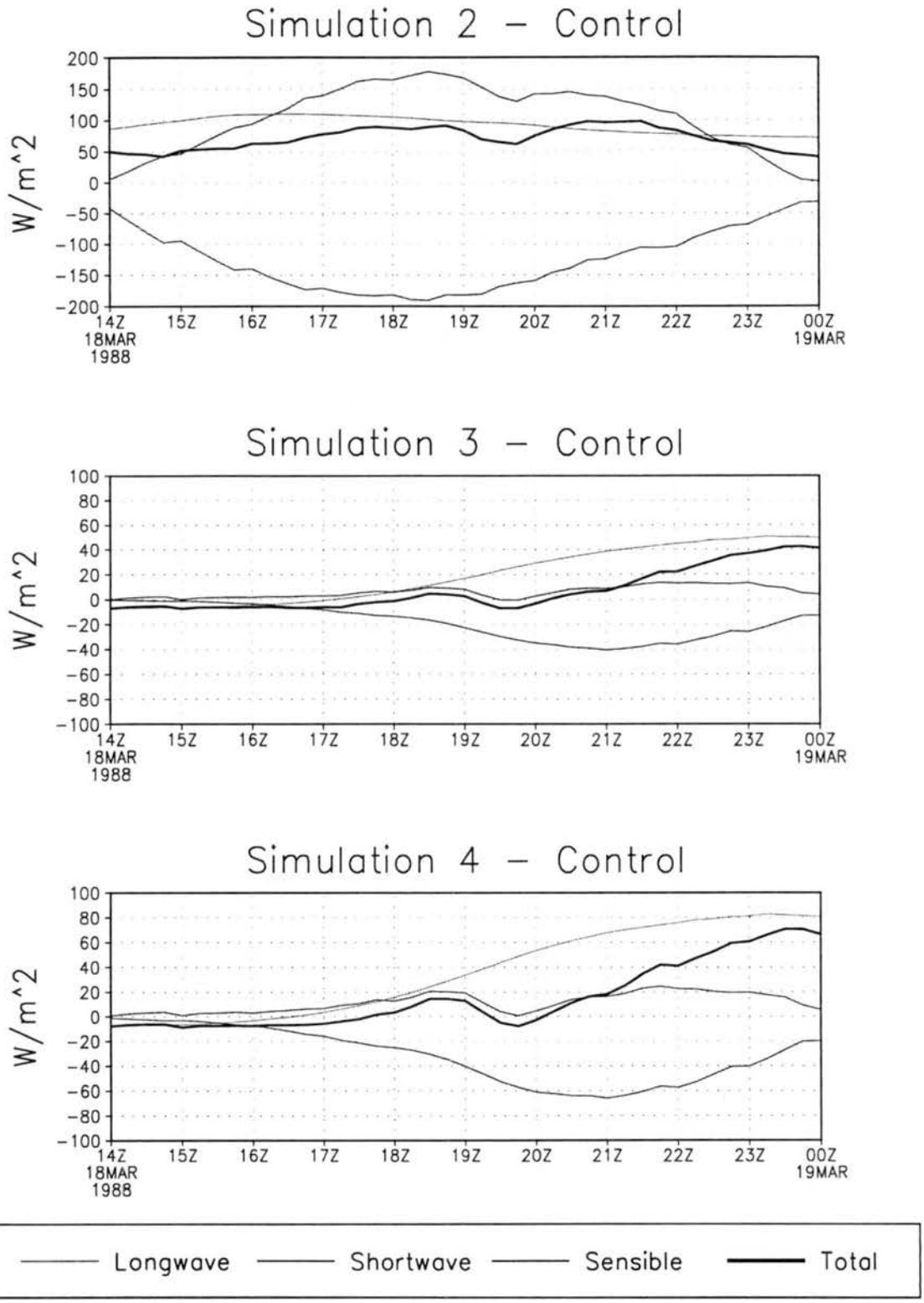

Figure 4.14: The differences in longwave, shortwave, and sensible heat fluxes absorbed by the snow from the control run for each of the simulations over region 1. These values were obtained by subtracting the area-averaged control run values from the area-averaged values for the other three simulations. The longwave radiation includes components from both the atmosphere and the vegetation.

near the surface. Above about 1000 m there is little difference between the two simulations which illustrates that the land-cover effects are most significant near the surface.

4.2.2 Region 2

Looking at Figures 4.9 and 4.11 it is seen that in simulation 2 the grass has been replaced with shrubs in region 2. Also, this land-cover set has a slightly larger area of crop land in region 2 than does the Landsat data set. From the canopy heights listed in Table 3.2 it can be seen that over most areas in region 2 there is now more protruding vegetation because of the shrubs. The average snow depth at initialization time in region 2 is about 0.25 m. This means that in the control run all the vegetation on average would have been buried. In contrast, in simulation 2 protruding shrubs cover over 80 percent of some grid cells in region 2.

The results of this land-cover change in region 2 are similar to those just discussed for region 1. This is to be expected since in both regions the primary effect of the land-cover change is to increase the coverage of protruding shrubs at the expense of shorter grass and crop stubble. Figure 4.16 shows that the sensible heat flux in simulation 2 increases much more rapidly during the morning hours and reaches a higher peak value than in the control run. The bottom panel shows that the latent heat flux is also much greater in simulation 2 than in the control run. This is likely due to the same reasons described for region 1. The top panel of Figure 4.17 shows that the air temperature is warmer during the morning as expected. The bottom panel of Figure 4.17 shows the more rapid snowmelt in simulation 2 over region 2. Looking at Figure 4.18, we see that the differences in the total and individual energy terms follow a similar pattern as in the case of region 1. There is an overall increase in the total amount of energy absorbed by the snow in simulation 2 which explains the more rapid snowmelt. Finally, Figure 4.19 shows a warmer and deeper boundary layer in simulation 2.

4.3 Simulation 3

In this simulation the AVHRR-derived land cover is used with the OGE grass/shrub mixture defined as all grass as is done by default in RAMS 4.30. The main effect of

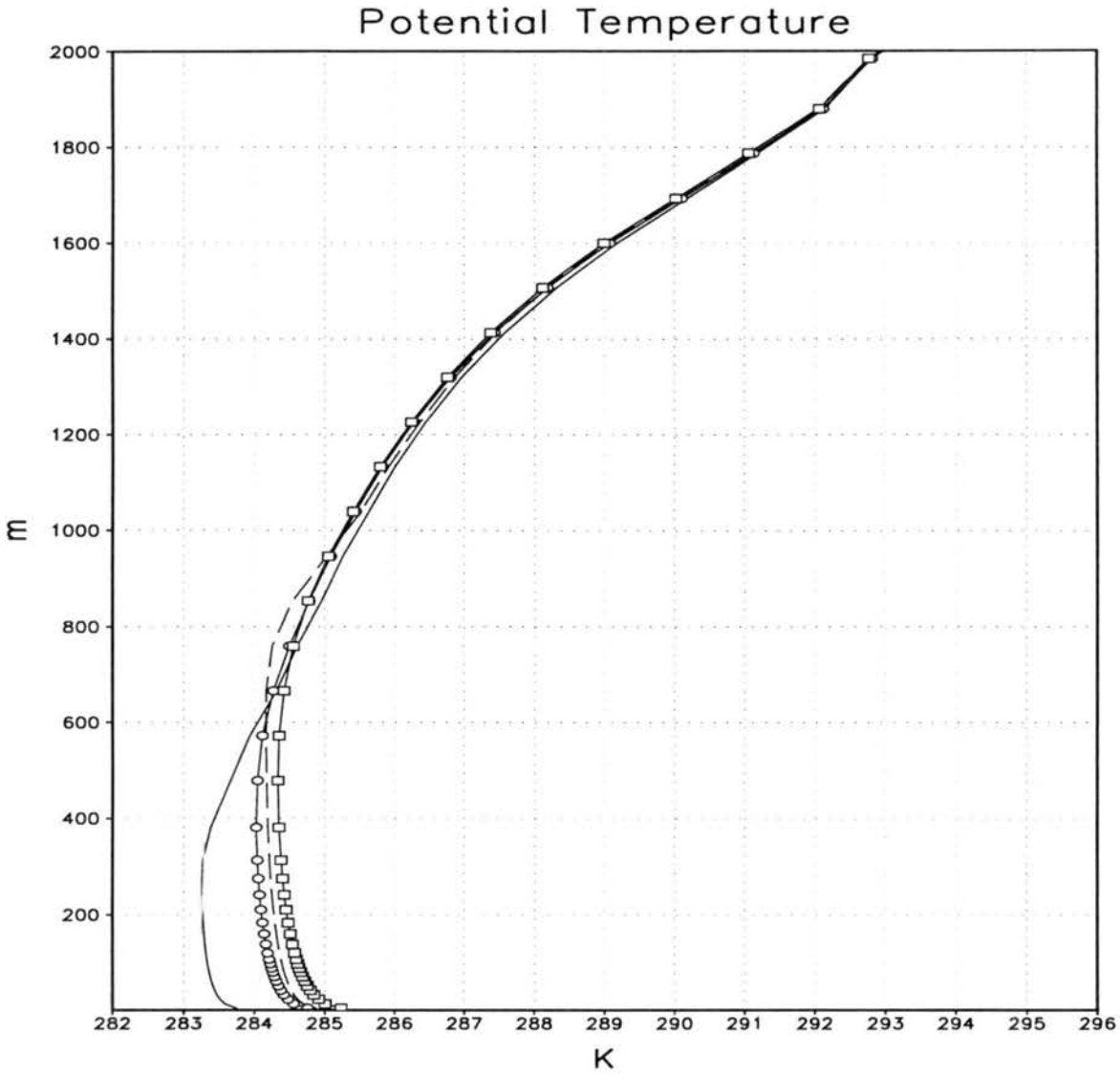

Figure 4.15: Area-averaged 2100 UTC potential temperature profile for region 1. Solid line is for control run, dashed line for simulation 2, line with circles is for simulation 3, and line with squares is for simulation 4.

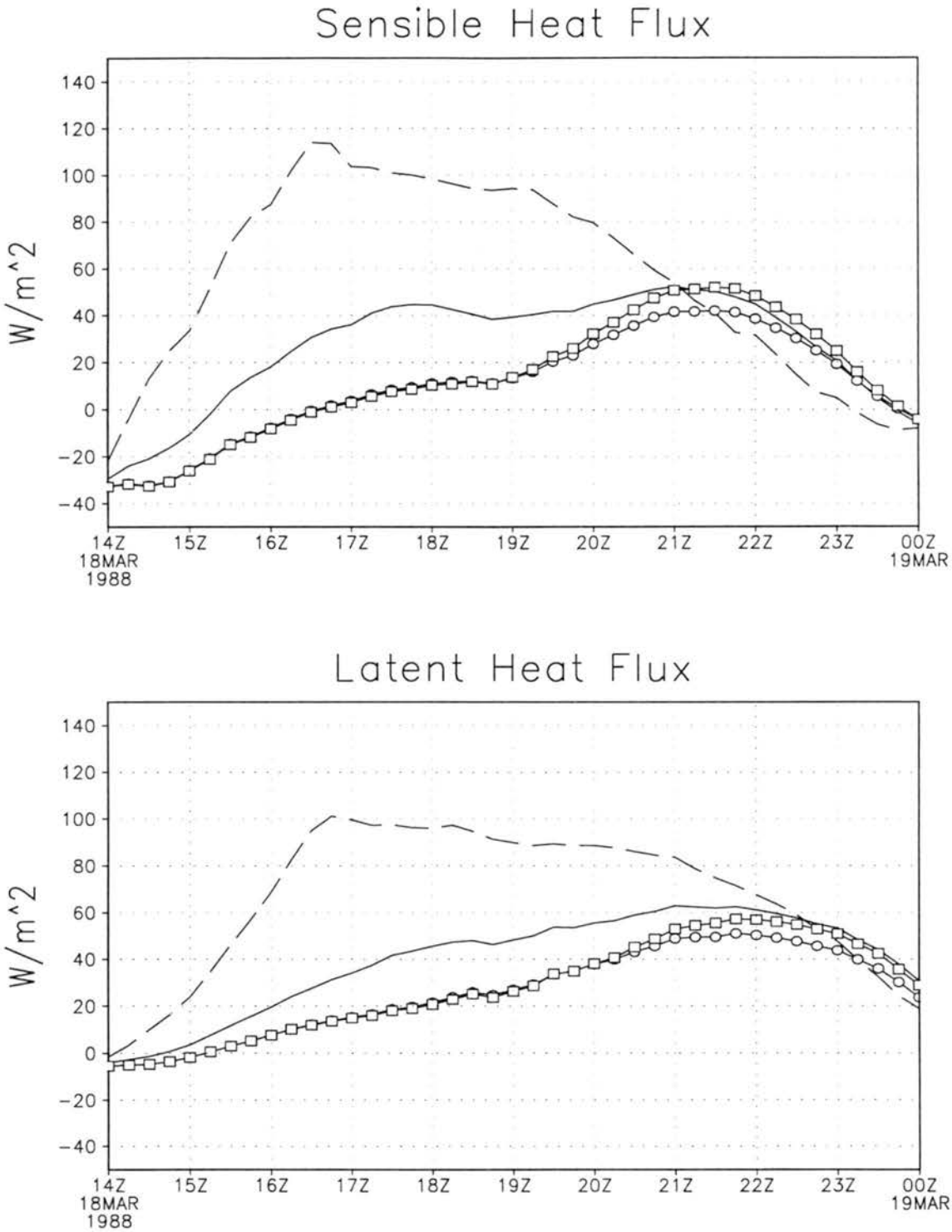

Figure 4.16: Area-averaged sensible and latent heat fluxes over region 2. Solid line is for control run, dashed line for simulation 2, line with circles is for simulation 3, and line with squares is for simulation 4.

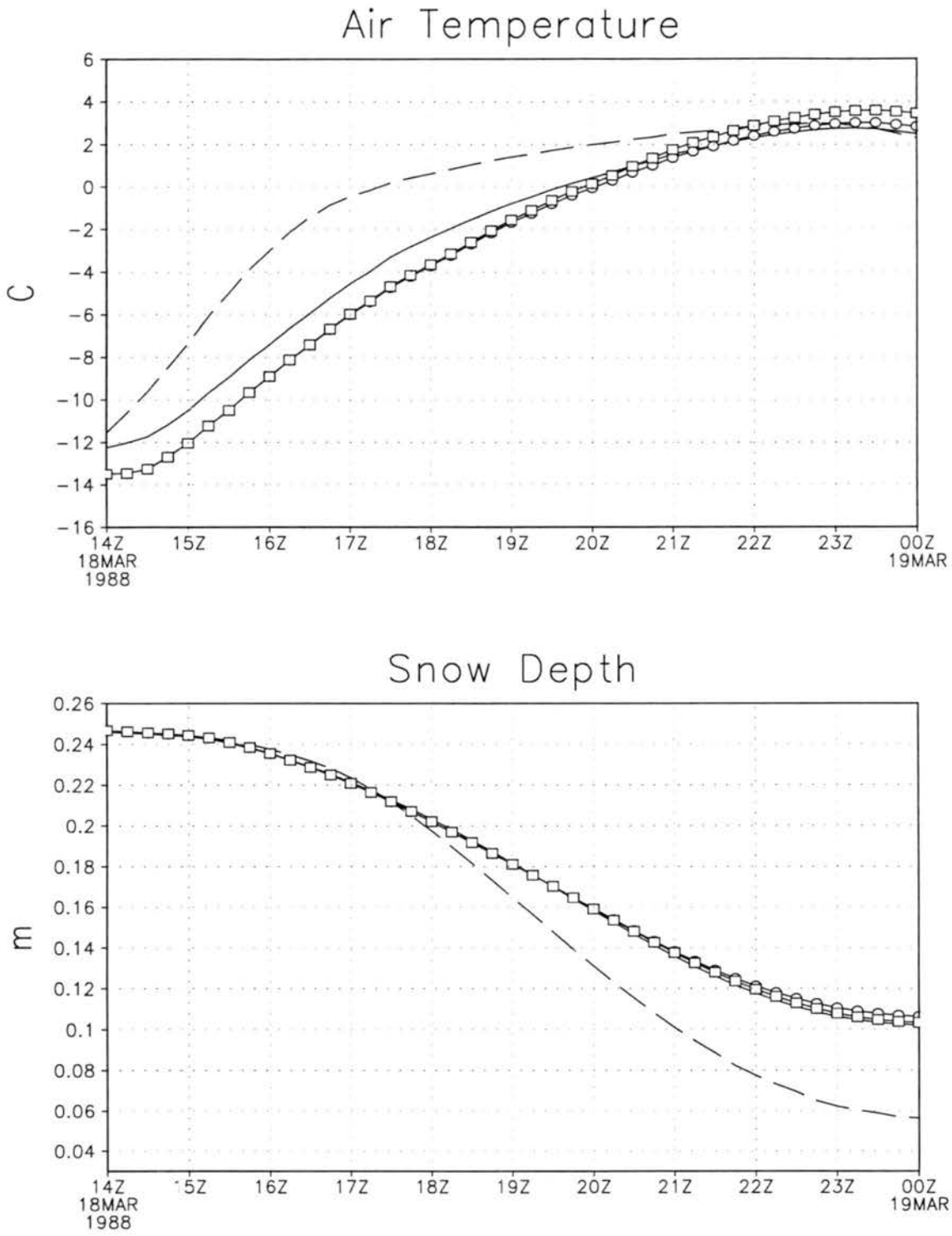

Figure 4.17: Area-averaged 5 m temperature and snow depth over region 2. Solid line is for control run, dashed line for simulation 2, line with circles is for simulation 3, and line with squares is for simulation 4.

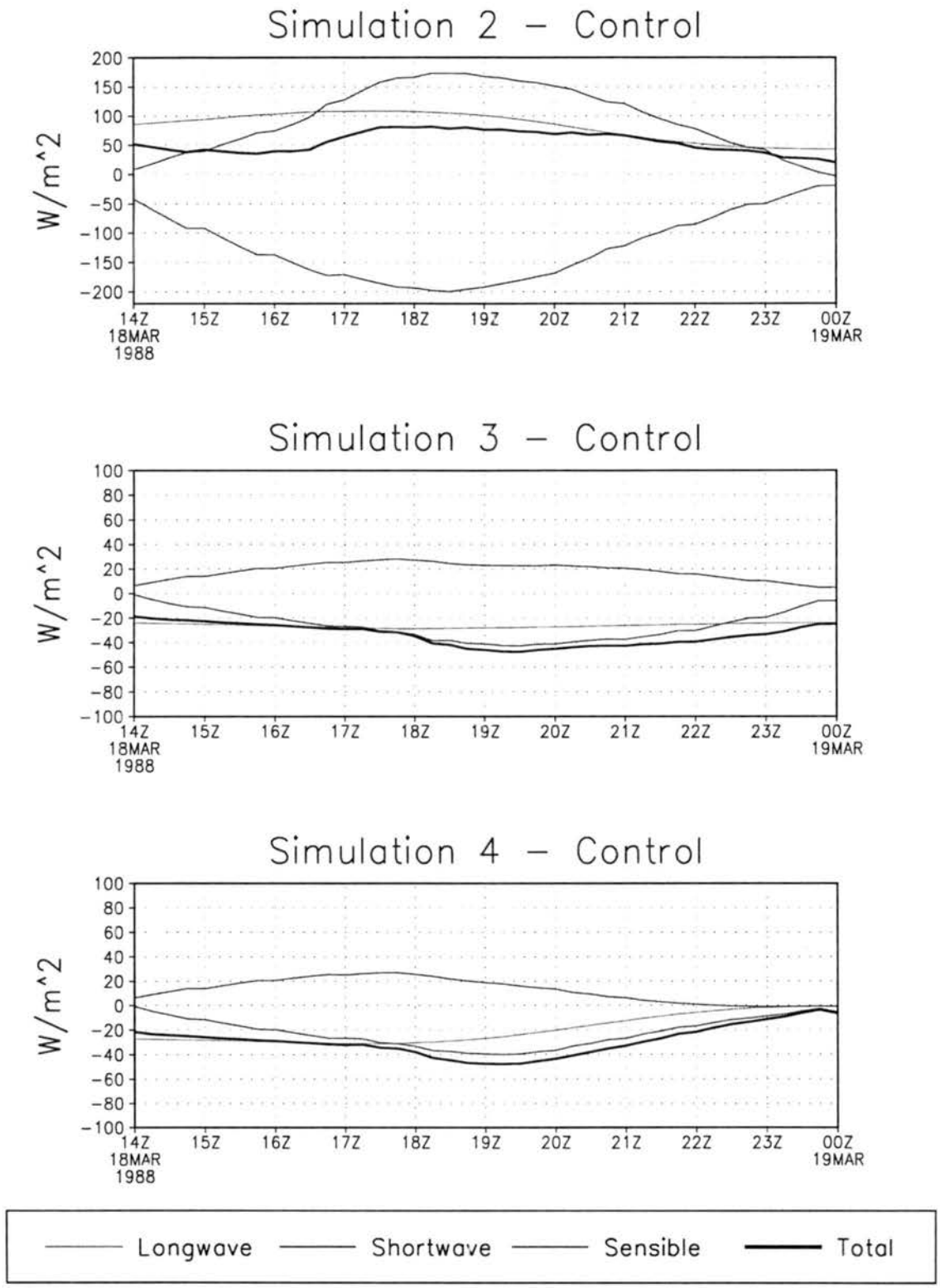

Figure 4.18: Same as Figure 4.14 except for region 2.

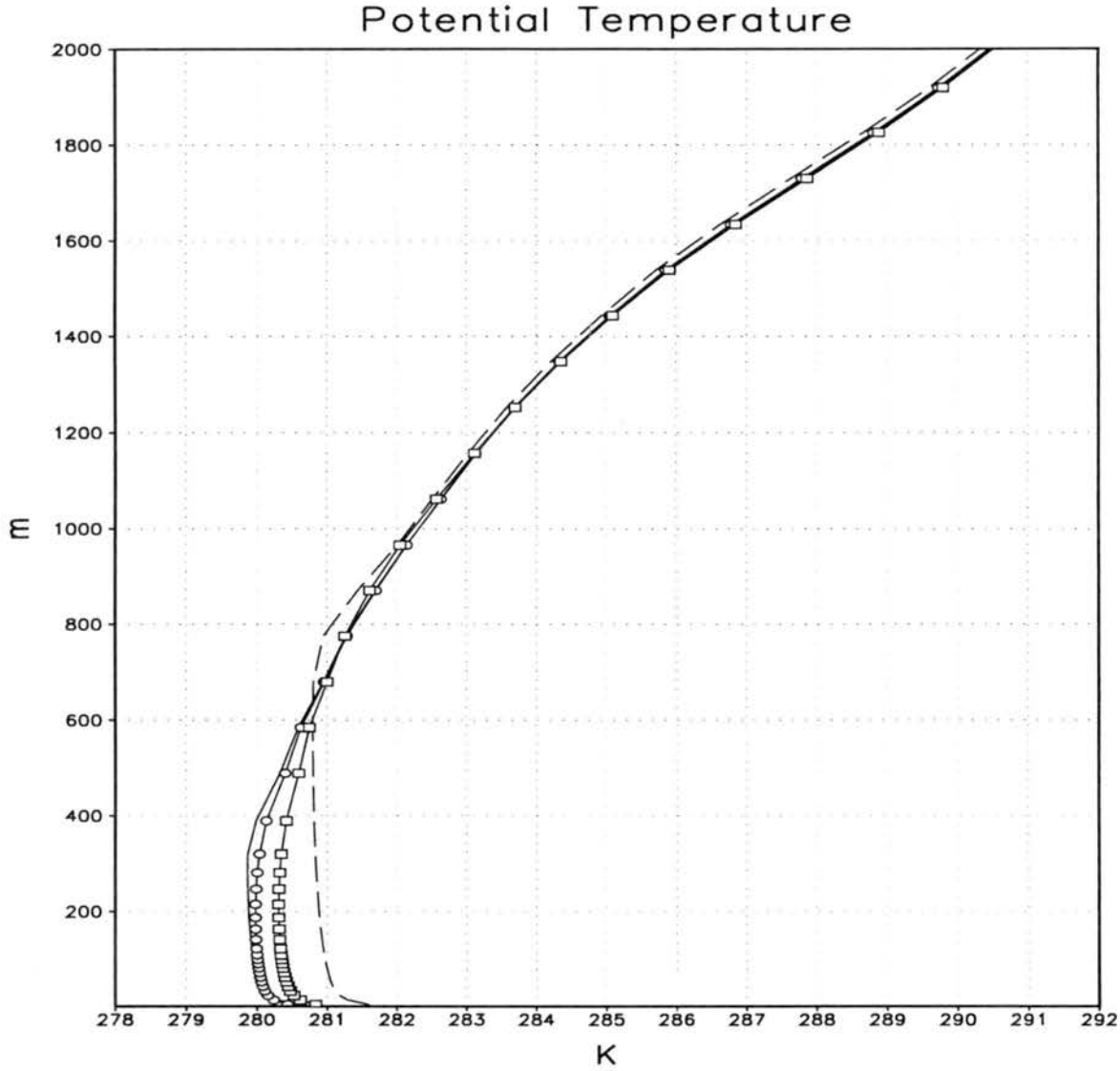

Figure 4.19: Area-averaged 2100 UTC potential temperature profile for region 2. Solid line is for control run, dashed line for simulation 2, line with circles is for simulation 3, and line with squares is for simulation 4.

this change in region 1 is to increase the amount of grass at the expense of crop stubble and winter wheat; see Figures 4.8 and 4.20. The changes in region 2 are slight in this simulation with only a small increase in crop areas and the removal of the small shrub fraction that was present in the Landsat data; see Figure 4.21. The effects of these changes on the surface heat fluxes, air temperature, snow depth, and boundary-layer structure are discussed below.

4.3.1 Region 1

Since the land-cover change in this simulation has increased the amount of protruding vegetation in region 1 higher sensible heat fluxes are expected. The top panel of Figure 4.12 shows that this is the case. The average snow depth at model start time in region 1 is 0.19 m meaning the grass with canopy height of 0.2 m protrudes slightly. In the control run there is more crop stubble and winter wheat which is assumed to have canopy heights of 0.05 and 0.1 m respectively. This vegetation is easily masked at the start of the simulation. Figure 4.12 shows that the maximum surface sensible heat flux in this case is about 40 W m^{-2} higher in simulation 3 than in the control run. The bottom panel of Figure 4.12 shows that the latent heat flux peaks about 20 W m^{-2} higher in simulation 3 than in the control run. The surface sensible and latent heat fluxes for simulation 3 are both less than those in simulation 2, reflecting the smaller volume of protruding material in simulation 3. The top panel of Figure 4.13 shows that the maximum daytime temperature peaks about 1°C higher than in the control run. In this case there is not much difference in snowmelt as shown by the curves in the bottom panel of Figure 4.13. From Figure 4.14 we see that for most of the day there is little difference in the total absorbed energy between simulation 3 and the control run. Finally, it can be seen in Figure 4.15 that the higher sensible heat flux does deepen and warm the boundary layer some.

4.3.2 Region 2

By removing the shrubs and increasing crop land the amount of protruding vegetation in this case has been reduced. The effects of this on the sensible heat flux is shown in the top panel of Figure 4.16. The sensible heat flux does not increase as rapidly in the morning

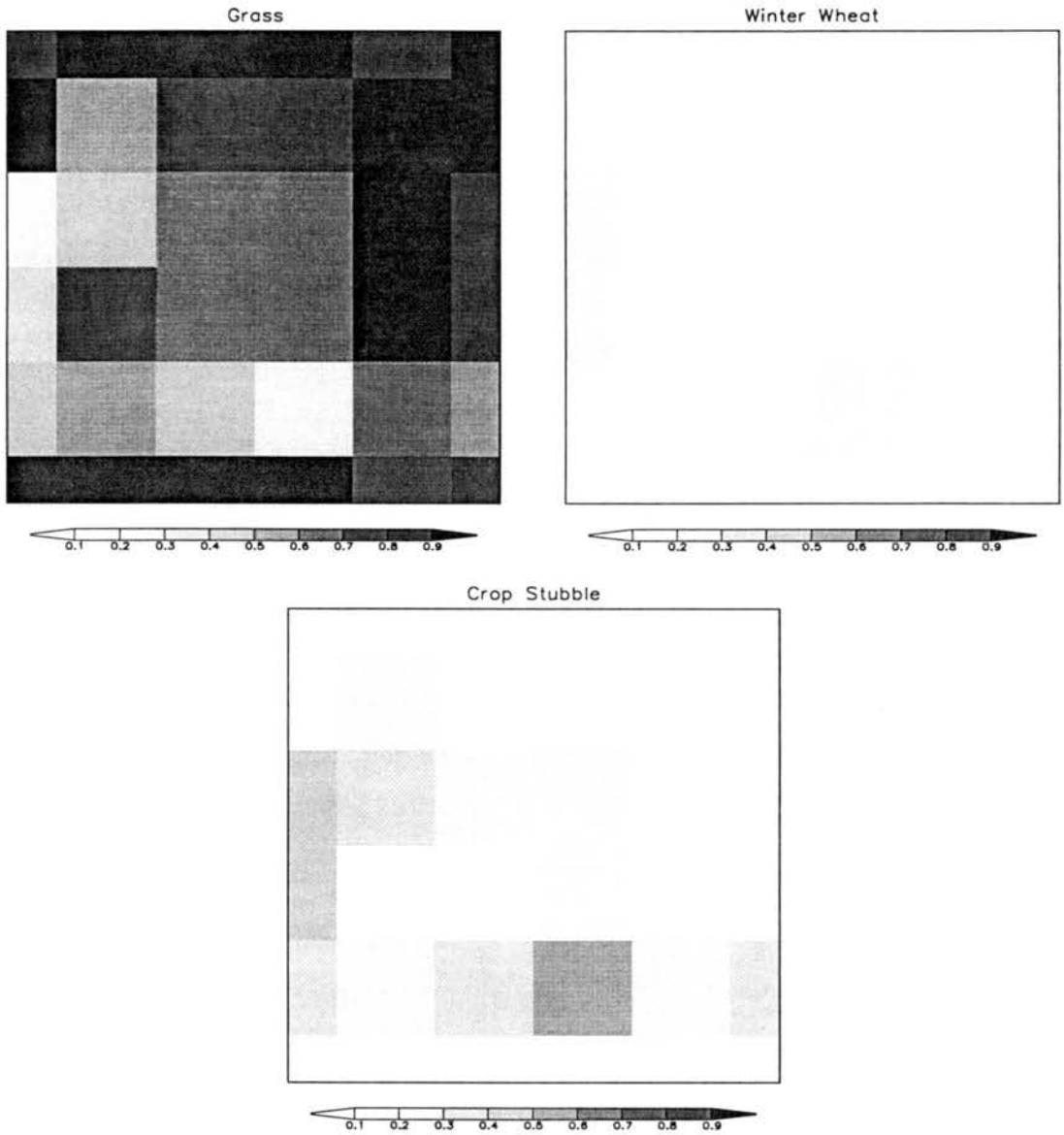

Figure 4.20: Fraction of each grid cell in region 1 that is occupied by the major land-cover categories as determined from the AVHRR data with the shrub/grass mixture defined as all grass.

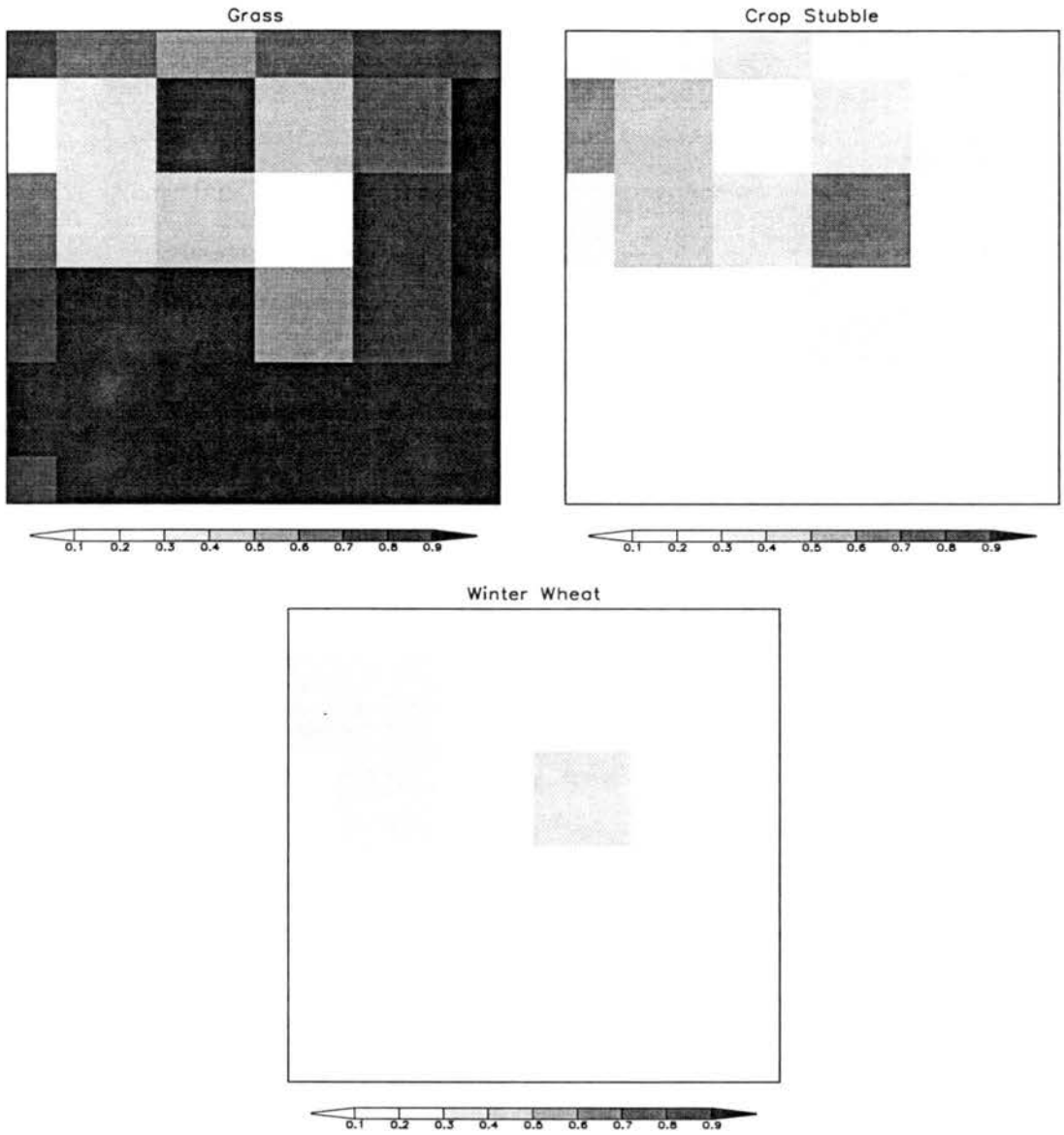

Figure 4.21: Same as for Figure 4.20 except for region 2.

and peaks slightly lower than in the control run. The latent heat flux is similarly reduced as shown in the bottom panel of Figure 4.16. The reduction in sensible heat flux leads to a slight decrease in morning air temperatures as shown in the top panel of Figure 4.17. The bottom panel of Figure 4.17 shows that there is only a slight decrease in snowmelt in this case. Figure 4.18 shows that the total amount of longwave, shortwave, and sensible heat fluxes absorbed by the snow is slightly less in simulation 3 than in the control run. The amount of shortwave radiation absorbed is greater in simulation 3 because there is less protruding vegetation to shade the surface. However, the reductions in longwave and sensible heat fluxes more than offset the increase in solar radiation leading to a net decrease in the amount of energy absorbed by the snow in simulation 3. From Figure 4.19 it is seen that there is also little difference in boundary-layer temperature and depth.

4.4 Simulation 4

In simulation 4 the land cover is defined entirely as short grass, a condition that represents the natural state of the land in this region. An examination of Figure 4.8 shows that a significant amount of the short grass in region 1 has been replaced with crop land that is either in stubble or winter wheat in late March. Figure 4.9 shows that region 2 still consists predominantly of short grass, but shrubs have increased in the southern areas and crop land has increased in the northern areas.

4.4.1 Region 1

In simulation 4 the short grass with canopy height of 0.2 m will protrude to some extent from the snow over much of region 1. In contrast, the present day crop stubble and winter wheat in the control run will be completely masked. From the top panel of Figure 4.12 it is seen that the maximum sensible heat flux is nearly 70 W m^{-2} larger in the natural case, simulation 4, than in the control run. The maximum latent heat flux, shown in the bottom panel of Figure 4.12, is about 40 W m^{-2} larger in the natural simulation. These results are consistent with the greater amount of protruding vegetation in the natural case.

Figure 4.13 shows that the air temperature is nearly 2°C warmer in simulation 4 than in the control run by late afternoon. The average snow depth is also slightly less in simulation 4 than in the control run by late afternoon; shown in the bottom panel of Figure 4.13. This is consistent with the increased amount of energy absorbed by the snow in simulation 4; see Figure 4.14. Figure 4.15 shows that the boundary layer in simulation 4 is about 1 K warmer and 200-300 m deeper than in the control run.

4.4.2 Region 2

In this region the average snow depth at initialization time is 0.25 m meaning the crop land and grass will be completely masked and only the shrubs will protrude. Since in simulation 4 there are no shrubs the surface is completely masked over all of region 2. In the control run, which has the present day land cover, shrubs exist in the southern portion of region 2; see Figure 4.9. Taking this into consideration one would expect that higher sensible heat fluxes and air temperatures would be expected in the present day case than in the all short grass condition.

A look at Figure 4.16 shows that the sensible heat flux is smaller in the natural case during the morning, but is actually slightly larger by late afternoon. The larger late afternoon sensible heat flux probably occurs because by this time the snow depth has decreased below the height of the grass over much of region 2. Since the natural case has all grass, while the present day case has some crop land, there is now more protruding vegetation in the natural case. Figure 4.16 also shows that the latent heat flux is less in the natural case than in the present day situation. The air temperature is cooler in the natural simulation during the morning and early afternoon then becomes slightly warmer by late afternoon; see Figure 4.17. This is consistent with the pattern of sensible heat flux. The bottom panel of Figure 4.17 shows that there is a slight reduction in snowmelt in the case with natural cover which is consistent with the reduction in total energy absorbed by the snow; see Figure 4.18. Finally, Figure 4.19 shows that the boundary layer is slightly warmer in the natural case by mid-afternoon, but there is little difference in depth. This is not what is expected since the surface sensible heat flux is less in the natural case up until the time of the profile. One possible explanation is horizontal advection. The

low-level winds are from the west and northwest during the hours before the time of the profile. In the control run a region of crop stubble and winter wheat is located to the west and northwest of region 2. Advection from this crop area, where there is less protruding vegetation, would help to cool the profile over region 2 in the control run. In contrast, in the natural case the taller grass begins to protrude by late morning increasing the local surface heating and thus reducing the advection of colder air into region 2.

Chapter 5

CONCLUDING REMARKS

5.1 Summary and Conclusions

The ability of snow to suppress daytime temperatures depends upon the degree to which it is able to mask the land cover. Protruding vegetation absorbs solar radiation, warms, and emits upward turbulent heat flux. This will lead to higher air temperatures and a deeper boundary layer. In contrast, lower temperatures will occur over a region where snow completely buries the vegetation and limits the surface temperature to 0°C. This means that the accuracy of daytime air temperatures simulated by a model will be dependent upon how representative the land cover in the model is.

In this study we have investigated the sensitivity of RAMS-generated surface sensible and latent heat fluxes, air temperature, snowmelt rate, and boundary-layer structure to the land-cover representation used. A control simulation was first performed using the best representation of the current landscape. The results of this control were verified against observations from ground stations and the SSBLIM aircraft. Three additional simulations, each with a different land-cover representation, were then run and the results compared with the control run.

In simulation 2 the AVHRR-derived land cover was used with the Olson grass/shrub mixture defined as all shrubs. This change led to much higher sensible heat fluxes and air temperatures over a region that was predominantly crops in the control run. Similar results were found for a region that was mainly grass in the control run. The primary effect of this land-cover change was to increase the amount of protruding vegetation in both of the study regions. In simulation 3 the same AVHRR-derived land cover was also used, but with the Olson grass/shrub class defined as all grass. This produced sensible

heat fluxes and air temperatures higher than in the control run but less than in simulation 2 over the predominantly crop area (region 1). The grass in this case protrudes more than the crop stubble and winter wheat but less than the shrubs. Slightly lower sensible heat fluxes and air temperatures occurred over region 2 since the area of crops was slightly larger there in simulation 3. Finally, simulation 4 suggests that converting natural grass land in the Texas Panhandle to crop stubble and winter wheat may lead to cooler daytime temperatures over snow while increased shrubs may lead to warmer temperatures. In region 1, which is mostly crop land at the present, higher sensible heat fluxes and air temperatures were simulated when the land cover was changed to its natural state. In contrast, in region 2, which has some shrubs at the present, lower sensible heat fluxes and air temperatures were simulated when the land cover was changed to its natural state.

The results of this study help to shed light on how sensitive models such as RAMS are to the land-cover representation. From the earlier discussion we can see that the choice of land-cover data can lead to differences in temperature over snow by as much as 6°C. The height of the afternoon boundary layer over snow can also vary by as much as several hundred meters when different land-cover data sets are used. In addition, the last simulation suggests that anthropogenic land-use change can have a significant impact on local temperatures over snow during the day. This study should point to the need for modelers to exercise care in defining the land cover for weather and climate simulations. The results also illustrate that in simulations of long-term climate a model should be able to predict and represent changes in vegetation patterns. Finally, this study also shows how important it is for weather and climate models to be able to reasonably simulate the evolution of snow depth. If the model can not accurately simulate changes in snow depth then it will not have the proper fractions of exposed vegetation and snow and thus will incorrectly simulate the surface heat balance.

5.2 Suggestions for Future Work

An obvious extension of this work would be to run a seasonal simulation over the northern U.S. Great Plains during winter. This region has undergone many of the same

changes in land-use that the Texas Panhandle has, namely introduction of crops and increased woody species in the remaining grass areas. Since snow covers the ground for a larger part of the winter in this region the daily effects described above will likely add up and produce significantly different seasonal average temperatures and snowmelt rates. There may also be significant differences in average precipitation since the alterations to the surface heat fluxes will influence the boundary-layer stability.

Lastly, some improvements to LEAF-2 should be considered. These include basing the sensible heat flux from the vegetation to the canopy air on a total area index instead of just the LAI and coupling with a plant model to dynamically generate values for LAI, vegetation fraction, canopy height, and albedo. As mentioned earlier in this text LEAF-2 calculates the sensible heat flux from the vegetation to the canopy using the LAI, which in this case is a measure of the green leaf area. In reality, the area of branches and dead leaves should also be included since these will warm and emit a turbulent flux as well. This problem is the worst for the case of deciduous species in winter since they will generate little or no heat flux in the current treatment when they are nearly bare of leaves.

Another improvement would be to couple LEAF-2 with a dynamic plant model, such as GEMTM (Chen and Coughenour 1994) or CENTURY (Parton 1996). These models could be used to prognose LAI, vegetation fraction, canopy height, and albedo from temperature, precipitation, solar radiation, etc. predicted by RAMS. These dynamic vegetation parameters could then be fed into LEAF-2 for calculating the various surface fluxes back to RAMS. This would be an improvement, especially for longer-term climate simulations, over the current situation where LEAF-2 prescribes over simplified seasonal variations to LAI and vegetation fraction and holds the other parameters constant.

REFERENCES

Baker, D.G., D.L. Ruschy, R.H. Skaggs, and D.B. Wall, 1992: Air temperature and radiation depressions associated with a snow cover. *J. Appl. Meteor.*, **31**, 247-254.

Beven, K.J., 1982: On subsurface stormflow, an analysis of response times. *Hydrol. Sci. J.*, **27**, 505-521.

Beven, K.J., and M.J. Kirkby, 1979: A physically based, variable contributing area model of basin hydrology. *Hydrol. Sci. Bull.*, **24**, 43-69.

Chen, C. and W.R. Cotton, 1983: A one-dimensional simulation of the stratocumulus-capped mixed layer. *Bound.-Layer Meteor.*, **25**, 289-321.

Chen, D.-X., and M.B. Coughenour, 1994: GEMTM: A general model for energy and mass transfer of land surfaces and its application at the FIFE sites. *Agric. Forest Meteor.*, **68**, 145-171.

Cohen, J., and D. Rind, 1991: The effect of snow cover on climate. *J. Climate*, **4**, 689-706.

Cramer, J., 1988: Observational evaluation of snow cover effects on the generation and modification of mesoscale circulations. Atmospheric Science Paper No. 439, Colorado State University, Fort Collins, CO.

Dickinson, R.E., A. Henderson-Sellers, P.J. Kennedy, and M.F. Wilson, 1986: Biosphere-Atmosphere Transfer Scheme (BATS) for the NCAR Community Climate Model. Technical Report NCAR/TN-275+STR, National Center for Atmospheric Research, Boulder, Colorado, USA.

Ellis, A.W., and D.J. Leathers, 1998: A quantitative approach to evaluating the effects of snow cover on cold airmass temperatures across the U.S. Great Plains. *Wea. Forecast.*, **13**, 688-701.

Greene, E.M., G.E. Liston, and R.A. Pielke, Sr., 1999: Relationships between landscape, snowcover depletion, and regional weather and climate. *Hydrol. Proc.*, **13**, 2453-2466.

Hartmann, D.L., 1994: *Global physical climatology.* Academic Press, San Diego, 411 pp.

Hatch, S.L. and J. Pluhar, 1993: *Texas range plants.* Texas A&M University Press, College Station, TX, 326 pp.

Huang, J., H.M. Van Den Dool, and K.P. Georgakakos, 1996: Analysis of model-calculated soil moisture over the United States (1931-1993) and applications to long-range temperature forecasts. *J. Climate*, **9**, 1350-1362.

Jones, O.R., and T.W. Popham, 1997: Cropping and tillage systems for dryland grain production in the southern high plains. *Agron. J.*, **89**, 222-232.

Kalnay, E., M. Kanamitsu, R. Kistler, W. Collins, D. Deaven, L. Gandin, M. Iredell, S. Saha, G. White, J. Woollen, Y. Zhu, M. Chelliah, W. Ebisuzaki, W. Higgins, J. Janowiak, K.C. Mo, C. Ropelewski, J. Wang, A. Leetmaa, R. Reynolds, R. Jenne, and D. Joseph, 1996: The NCEP/NCAR 40-year reanalysis project. *Bull. Amer. Meteor. Soc.*, **77**, 437-471.

Kou, H.L., 1968: The thermal interaction between the atmosphere and the earth and propagation of diurnal temperature waves. *J. Atmos. Sci.*, **25**, 682-706.

Leathers, D.J., and D.A. Robinson, 1993: The association between extremes in North American snow cover extent and United States temperatures. *J. Climate*, **6**, 1345-1355.

Lee, T.J., 1992: The impact of vegetation on the atmospheric boundary layer and convective storms. Atmospheric Science Paper No. 509, Dept. of Atmos. Sci., Colorado State Univ., Fort Collins, CO.

Louis, J.F., M. Tiedke, and J.-F. Geleyn, 1981: A short history of the PBL parameterization at the ECMWF. *Workshop on Planetary Boundary Layer Parameterization*, Shinfield Park, Reading, United Kingdom, ECMWF, 59-80.

Mellor, G.L., and T. Yamada, 1982: Development of a turbulence closure model for geophysical fluid problems. *Rev. Geophys. Space Phys.*, **20**, 851-871.

Namias, J., 1985: Some empirical evidence for the influence of snow cover on temperature and precipitation. *Mon. Wea. Rev.*, **113**, 1542-1553.

Olson, J.S., 1994a: Global ecosystem framework-definitions: USGS EROS Data Center Internal Report, Sioux Falls, SD, 37 pp.

Olson, J.S., 1994b: Global ecosystem framework-translation strategy: USGS EROS Data Center Internal Report, Sioux Falls, SD, 39 pp.

Otterman J., M.D. Novak, and D. O'C. Starr, 1993: Turbulent heat transfer from a sparsely vegetated surface: Two-component representation. *Bound.-Layer Meteor.*, **64**, 409-420.

Parton, W.J., 1996: The CENTURY model. NATO ASI Series, Vol. I38, Evaluation of Soil Organic Matter Models, D.S. Powlson, P. Smith, and J.U. Smith, Eds., Springer-Verlag, Berlin Heidelberg, 283-291.

Pielke, R.A., 2001: *Mesoscale meteorological modeling*, 2nd Ed., Academic Press, San Diego, CA.

Pielke, R.A., W.R. Cotton, R.L. Walko, C.J. Tremback, W.A. Lyons, L.D. Grasso, M.E. Nicholls, M.D. Moran, D.A. Wesley, T.J. Lee, and J.H. Copeland, 1992: A com-

prehensive meteorological modeling system – RAMS. *Meteor. Atmos. Phys.*, **49**, 69-91.

Sellers, W.D., 1965: *Physical climatology.* University of Chicago Press, IL, 272 pp.

Scifres, C.J., 1980: *Brush management: Principles and practices for Texas and the Southwest.* Texas A&M University Press, College Station, TX, 360 pp.

Shul'gin, A.M., 1965: The temperature regime of soils. Sivan Press, Jerusalem, Israel, 218 pp.

Sivapalan, M., K. Beven, and E.F. Wood, 1987: On hydrologic similarity: 2. A scaled model of storm runoff production. *Water Resour. Res.*, **23**, 2266-2278.

Smagorinsky, J., S. Manabe, and J.L. Holloway, Jr., 1965: Numerical results from a nine-level general circulation model of the atmosphere. *Mon. Wea. Rev.*, **93**, 727-798.

Thomas, G. and P.R. Rowntree, 1992: The boreal forests and climate. *Quart. J. Roy. Meteor. Soc.*, **118**, 469-497.

Viterbo, P. and A.K. Betts, 1999: Impact on ECMWF forecasts of changes to the albedo of the boreal forests in the presence of snow. *J. Geophys. Res.*, **104**, 27803-27810.

Vogelmann, J.E., T.L. Sohl, P.V. Campbell, and D.M. Shaw, 1998: Regional land cover characterization using Landsat Thematic Mapper Data and ancillary data sources. *Environ. Monitoring Assessment*, **51**, 415-428.

Walko, R.L., L.E. Band, J. Baron, T.G.F. Kittel, R. Lammers, T.J. Lee, D.S. Ojima, R.A. Pielke, C. Taylor, C. Tague, C.J. Tremback, and P.L. Vidale, 2000: Coupled atmosphere-biophysics-hydrology models for environmental modeling. *J. Appl. Meteor.*, **39**, 931-944.